Navigating the Waters of Unconventional Crystalline Hydrates
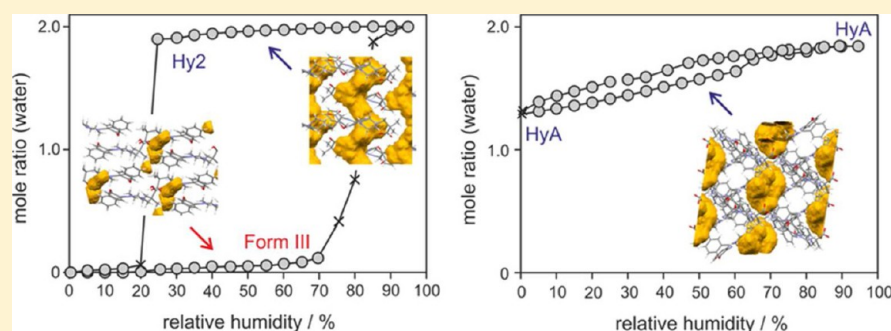
Doris E. Braun,*[†] Lien H. Koztecki,[§] Jennifer A. McMahon,[§] Sarah L. Price,[‡] and Susan M. Reutzel-Edens[§]

[†]Institute of Pharmacy, University of Innsbruck, Innrain 52c, 6020 Innsbruck, Austria
[‡]Department of Chemistry, University College London, 20 Gordon Street, London WC1H 0AJ, U.K.
[§]Eli Lilly and Company, Indianapolis, Indiana 46285, United States

S *Supporting Information*

ABSTRACT: Elucidating the crystal structures, transformations, and thermodynamics of the two zwitterionic hydrates (Hy2 and HyA) of 3-(4-dibenzo[b,f][1,4]oxepin-11-yl-piperazin-1-yl)-2,2-dimethylpropanoic acid (DB7) rationalizes the complex interplay of temperature, water activity, and pH on the solid form stability and transformation pathways to three neutral anhydrate polymorphs (Forms I, II°, and III). HyA contains 1.29 to 1.95 molecules of water per DB7 zwitterion (DB7^z). Removal of the essential water stabilizing HyA causes it to collapse to an amorphous phase, frequently concomitantly nucleating the stable anhydrate Forms I and II°. Hy2 is a stoichiometric dihydrate and the only known precursor to Form III, a high energy disordered anhydrate, with the level of disorder depending on the drying conditions. X-ray crystallography, solid state NMR, and H/D exchange experiments on highly crystalline phase pure samples obtained by exquisite control over crystallization, filtration, and drying conditions, along with computational modeling, provided a molecular level understanding of this system. The slow rates of many transformations and sensitivity of equilibria to exact conditions, arising from its varying static and dynamic disorder and water mobility in different phases, meant that characterizing DB7 hydration in terms of simplified hydrate classifications was inappropriate for developing this pharmaceutical.

KEYWORDS: hydrate, crystal polymorphism, proton transfer, crystal structure, electronic structure calculations, NMR prediction, thermal analysis, gravimetric moisture sorption/desorption, Raman spectroscopy, solid state NMR spectroscopy, hydrogen/deuterium exchange

1. INTRODUCTION

Water plays a critical role within pharmaceutical sciences. Introduced through the active ingredient, excipients, or the atmosphere, it can induce phase transitions, dissolve soluble components, and increase interactions between the drug and excipients, all of which can adversely affect the physical and chemical stability of the drug substance to the detriment of drug product performance. It must therefore be accounted for at all stages of drug substance and product manufacturing. Not surprisingly, of the many possible critical quality attributes of a drug substance, hygroscopicity, a measure of the water vapor taken up by a solid with the potential to effect surface and bulk properties, is routinely evaluated, typically by moisture sorption analysis, at the earliest stages of drug product development. The measurement of water vapor sorption isotherms must, however, be tied more directly to the mechanisms by which

water is taken up to truly understand the impact that water sorption has on the properties of the solid.[1]

On a molecular level, water has the ability to interact with a substance in many ways, including (i) physisorption or binding to the surface by hydrogen bonding, (ii) physical entrapment to form liquid inclusions, (iii) absorption in localized disordered regions, (iv) chemical addition,[2] and (v) hydrate formation.[3] Hydrates often crystallize because water improves crystal packing efficiency and satisfies the hydrogen bonding sites of the drug better than the drug itself.[3−9] Hydrates may be *stoichiometric* or *nonstoichiometric*.[3,10−13] Stoichiometric hy-

drates show step-shaped sorption/desorption isotherms characterized by a fixed water content over a defined relative humidity (RH) range and generally convert upon dehydration to a distinct phase, crystalline or amorphous. The waters of crystallization usually play a crucial role in stabilizing the molecular network. Nonstoichiometric hydrates,[14] however, have a continuously variable composition within a certain RH range that is not associated with a significant change in the crystal lattice, except for possibly anisotropic expansion of the network to accommodate water.[12] Dehydrating a nonstoichiometric hydrate may result in an isomorphic dehydrate (desolvate),[15−18] a one-component phase that exhibits the main structural features of its parent phase. Desolvated solvates are usually metastable and easily take up the original solvent or sometimes other solvents to minimize free volume (void space) in the crystal.[3,19] In some cases, nonstoichiometric hydrates lose crystallinity and become amorphous[20] when the very last water is forced out by extreme drying conditions.

Whether a crystalline hydrate is targeted as the delivery vehicle for a drug in the formulated product or designed around in favor of a neat form, the dehydration and rehydration processes of a hydrate forming system can be complex and difficult to control.[21−33] Hydrates are generally expected to be thermodynamically more stable, hence less soluble and slower to dissolve than anhydrate forms above the critical water activity for hydrate formation.[21,34,35] However, as particle size/shape distribution, specific surface area, and other surface properties heavily affect dissolution, a hydrate may dissolve faster than an anhydrate.[35−39] Additionally, some hydrates are intrinsically more soluble (less stable) in water than neat forms.[8] Such exceptions to the general solubility trend include LY334370 HCl,[40] N-{[(5S)-3-(4-{6-[(1R,5S)-6-cyano-3-oxabicyclo[3.1.0]hex-6-yl]pyridin-3-yl}phenyl)-2-oxo-1,3-oxazolidin-5-yl]methyl}acetamide,[41] LY156735 (a melatonin agonist),[42] and norfloxacin.[43−45] Norfloxacin is considered unusual because its more soluble hydrates are zwitterionic and at least one of its anhydrates is charge neutral.[32] In this case, the higher solubility of the hydrate can be readily attributed to the stronger hydration of the highly charged zwitterions relative to the uncharged molecule in the anhydrous form.[46]

Another compound that shows water-induced proton transfer to form zwitterionic hydrates is the 5-HT$_{2a}$ and H$_1$ inverse agonist, 3-(4-dibenzo[b,f][1,4]oxepin-11-yl-piperazin-1-yl)-2,2-dimethylpropanoic acid (LY2624803 or DB7, Figure 1). We previously used DB7 as a model compound to test the value of combining computational crystal structure prediction (CSP) methods with an industrial solid form screening program.[47] From the experimental screen for solid forms, which encompassed a broad range of crystallization conditions and totaled over 300 experiments, DB7 was identified in nine solid forms, including three neat polymorphs (Forms I−III), a stoichiometric dihydrate (Hy2), a nonstoichiometric hydrate (HyA), three unstable isostructural solvates (from methanol, ethanol, and 2-propanol), and an amorphous form. For an amphoteric molecule with measured pK_a values of 2.95 (oxepine-N), 4.03 (carboxylic acid), and 7.81 (piperidine-N), application of the pK_a rule of three would suggest that proton transfer from the carboxylic acid to the piperidine-N is essentially complete rendering DB7 zwitterionic, at least in aqueous solutions at moderate pH.[48] However, solid state ^{15}N NMR spectra provided an initial indication that only Hy2 and HyA contain zwitterions (DB7^z); the neat forms contain the neutral DB7 molecule.[47]
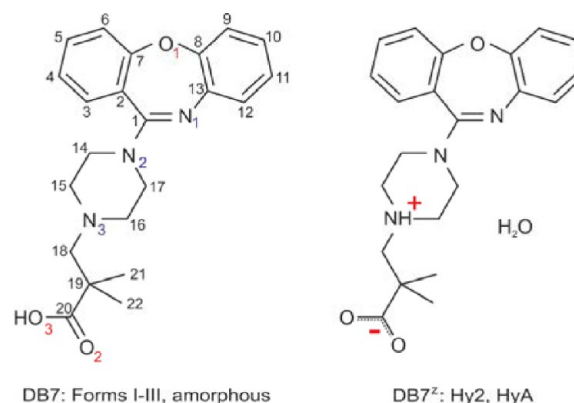

Figure 1. Molecular diagrams of DB7 in the charge neutral anhydrous Forms I−III and amorphous form and in the zwitterionic hydrates. The abbreviated name DB7 refers to the dibenzoxazepinyl ring system.[47] The atomic numbering given on the charge neutral form is also used for zwitterionic phases, which are indicated with superscript "z".

In this study, we explore through a combination of experiment and computation the structural and thermodynamic relationships[25,28,29,40,49−52] between the hydrate/anhydrate phases of DB7 and their interconversion pathways as a function of temperature, water activity, and pH. A range of experimental techniques, along with computed lattice energies and chemical shift prediction of experimental and hypothetical structures, are used to understand at an atomistic level[53−56] two distinct (de)hydration mechanisms of stoichiometric and nonstoichiometric hydrates complicated by both structural disorder and proton transfer.

2. EXPERIMENTAL SECTION

2.1. Materials and Preparation of DB7^z Hydrates. DB7 (Form II°, purity 99.6%) was obtained from Lilly Research Laboratories. The dihydrate (Hy2) was prepared by dissolving amorphous DB7 (prepared by rotovapping a dichloromethane solution of the compound) in stirred water (pH 5.9) at RT. Within 15 min a thick white slurry, Hy2, had formed. The solid product was isolated by vacuum filtration and dried in a 75% RH chamber. After stirring in water at RT for 10 days Hy2 transformed to the second hydrate (HyA). The solid product was isolated by vacuum filtration, washed/transferred with water, air-dried, and equilibrated for several days at 43% RH to further dry the sample. Experiments on Hy2 and HyA were performed with samples that had been stored at 75% RH over a saturated NaCl solution. For solubility experiments the hydrate samples were equilibrated at 92% RH (over a saturated KNO$_3$ solution), for SSNMR experiments at 75, 58, 43, 33, 22, and 11% RH and for H$_2$O/D$_2$O exchange (Raman) experiments at 98 and 11% RH.

The three anhydrates, Forms I−III, were prepared according to ref 47.

2.2. Single Crystal X-ray Diffractometry. Single crystal X-ray diffraction data were collected using a Bruker D$_8$-based 3-circle geometry diffractometer equipped with a CuKα (Hy2) or MoKα (HyA) radiation source and a SMART APEX II 6000 CCD area detector. Hy2 and HyA$_{1.95}$ crystals were taken freshly from the mother liquor and HyA$_{1.73}$ after storing the sample at ambient conditions (∼40% RH). Cell refinement and data reduction were accomplished using the SAINT software program.[57] The structures were solved by direct methods

Table 1. Crystallographic Data for DB7^z Hy2 and HyA

phase designator	Hy2	HyA$_{1.95}$	HyA$_{1.73}$
empirical formula	C$_{22}$H$_{25}$N$_3$O$_3$·2(H$_2$O)	C$_{22}$H$_{25}$N$_3$O$_3$·1.95(H$_2$O)	C$_{22}$H$_{25}$N$_3$O$_3$·1.73(H$_2$O)
formula weight	415.48	414.59	410.63
temperature/K	100	100	100
wavelength/Å	Cu $K\alpha$	Mo $K\alpha$	Mo $K\alpha$
crystal size/mm	0.20 × 0.10 × 0.05	0.30 × 0.21 × 0.20	0.14 × 0.12 × 0.06
crystal system	monoclinic	monoclinic	monoclinic
space group	$P2_1/c$	$C2/c$	$C2/c$
a/Å	13.212 (2)	26.663(7)	26.498(3)
b/Å	9.1505 (15)	9.634(2)	9.6469(3)
c/Å	18.160 (3)	20.863(9)	20.342(3)
α/deg	90	90	90
β/deg	105.195 (11)	128.322(6)	128.706(4)
γ/deg	90	90	90
volume/Å^3	2118.7(6)	4205(2)	4057.9(8)
Z	4	8	8
density (calc)/ g cm^{-3}	1.303	1.310	1.344
theta range for data collection/deg	3.47 to 64.75	1.95 to 25.75	1.97 to 24.72
index ranges	$-15 \leq h \leq 15$	$-23 \leq h \leq 32$	$-26 \leq h \leq 34$
	$-9 \leq k \leq 10$	$-11 \leq k \leq 8$	$-10 \leq k \leq 11$
	$-21 \leq l \leq 21$	$-25 \leq l \leq 17$	$-23 \leq l \leq 2$
No. of measured, independent, and observed $[I > 2\sigma(I)]$ reflections	15085/3575/2408	7816/3987/2331	8478/2810/1811
refinement method	full-matrix least-squares on F2	full-matrix least-squares on F2	full-matrix least-squares on F2
data/parameters/restraints	3575/294/14	3987/320/12	2810/321/12
R_{int}	0.125	0.037	0.046
goodness-of-fit	0.96 (on F2)	1.00 (on F2)	1.04 (on F2)
final R indices $[I > 2\mathrm{sigma}(I)]$	R1 = 0.0529	R1 = 0.0499	R1 = 0.0544
	wR2 = 0.1271	wR2 = 0.0978	wR2 = 0.1281
R indices (all data)	R1 = 0.0796	R1 = 0.1056	R1 = 0.0994
	wR2 = 0.1389	wR2 = 0.1217	wR2 = 0.1493
largest diff. peak and hole/eÅ^{-3}	0.65 and −0.46	0.29 and −0.21	0.22 and −0.24

using the program package WinGX[58] (SIR2011[59] and SHELXL2013[60]). All non-H atoms were refined anisotropically. The aromatic and aliphatic hydrogen atoms were generated by a riding model on idealized geometries with $U_{iso}(H) = 1.2U_{eq}(C)$ for aromatic and nonterminal aliphatic hydrogens and $U_{iso}(H) = 1.5U_{eq}(C)$ for −CH$_3$. Water hydrogen atoms and Hy2 N$^+$−H were located from the difference map and refined with constrained O/N$^+$−H bond distances and $U_{iso}(H) = 1.5U_{eq}(O)/U_{iso}(H) = 1.2U_{eq}(N)$. The HyA N$^+$−H proton was identified from the difference map and refined isotropically. Further details are provided in Table 1. Proton disorder of the Hy2 water molecules is addressed in Section 3.2.1 and HyA water position occupancies/disorder in Section 3.2.2. The structure models for both hydrates were supported with electronic structure calculations (Sections 11−16 of the Supporting Information).

2.3. X-ray Powder Diffractometry. XRPD patterns were obtained using an X'Pert PRO diffractometer (PANalytical, Almelo, NL) equipped with a theta/theta coupled goniometer in transmission geometry, programmable XYZ stage with well plate holder, Cu−K$\alpha_{1,2}$ radiation source with a focusing mirror, a 0.5° divergence slit and a 0.02° Soller slit collimator on the incident beam side, a 2 mm antiscattering slit and a 0.02° Soller slit collimator on the diffracted beam side, and a solid state PIXcel detector. The patterns were recorded at a tube voltage of 40 kV and tube current of 40 mA, applying a step size of 2θ = 0.013° with 40s/80s per step in the 2θ range between 2° and 40°. For nonambient RH measurements a VGI stage (VGI 2000M, Middlesex, U.K.) was used.

The diffraction patterns were indexed using the first 20 peaks with DICVOL04, and the space group, which was determined based on a statistical assessment of systematic absences[61] as implemented in the DASH structure solution package,[62] agreed with the single crystal data ignoring temperature effects. Pawley fits[63] and Rietveld refinements[64] were performed with Topas Academic V5.[65] The background was modeled with Chebyshev polynomials and the modified Thompson−Cox−Hastings pseudo-Voigt function was used for peak shape fitting. For the Rietveld refinements the DB7^z molecule was refined with restraints (distances, angles, and aromatic rings flattened) and the water molecules as oxygens only. Water positions W1$_A$ and W1$_B$ were modeled as one position.

2.4. Gravimetric Moisture Sorption/Desorption Experiments. Moisture sorption and desorption studies were performed with the automatic multisample gravimetric moisture sorption analyzer SPS23-10μ (ProUmid, Ulm, Germany). Approximately 100−200 mg of sample was used for each analysis. The measurement cycles were started at 40% with an initial stepwise desorption (decreasing humidity) to 0%, followed by a sorption cycle (increasing humidity) up to 95% and back to 0% relative humidity (RH). RH changes were set to 5% for all cycles. The equilibrium condition for each step was set to a mass constancy of ±0.001% over 60 min and a maximum time limit of 48 h for each step.

2.5. Calorimetry/Thermal Analysis.

Differential scanning calorimetry (DSC) was conducted using a TA Q1000 DSC, operated with Thermal Advantage Release 5.4.0 software (TA Instruments, USA) or a Diamond DSC equipped with a Controlled Cooling Accessory (Intracooler 1P) and operated with Pyris7.0 software (PerkinElmer, Norwalk, CT, USA). A few milligrams of accurately weighed (Mettler UM3 ultra-microbalance) sample was heated in perforated or sealed Al-pans. Heating rates ranging from 1 to 50 °C min^{-1} were applied with a nitrogen purge. The temperature and heat flow of the TA Q1000 were calibrated against indium melting. The Diamond DSC was calibrated for temperature with pure benzophenone (mp 48.0 °C) and caffeine (mp 236.2 °C), and the energy calibration was performed with indium (mp 156.6 °C, heat of fusion 28.45 J g^{-1}). The errors on the extrapolated transition onset temperatures and enthalpy values are 95% confidence intervals (CI) derived from at least three measurements.

Isothermal calorimetry was used to derive dehydration enthalpies (see Section 10 of the Supporting Information).

Thermogravimetric analysis (TGA) was carried out with a TGA7 system (PerkinElmer, USA) using Pyris 2.0 software. Approximately 2−5 mg of sample was weighed into a platinum pan. Two-point calibration of the temperature was performed with ferromagnetic materials (Alumel and Ni Curie-point standards, PerkinElmer). Heating rates ranging from 2 to 20 °C min^{-1} were applied, and dry nitrogen was used as a purge gas (sample purge, 20 mL min^{-1}; balance purge, 40 mL min^{-1}).

2.6. Spectroscopy.

Raman spectra were recorded with a Bruker RFS 100 Raman-spectrometer (Bruker Analytische Messtechnik GmbH, Germany), equipped with a Nd:YAG Laser (1064 nm) as the excitation source and a liquid-nitrogen-cooled, high sensitivity Ge-detector. The spectra (128 scans per spectrum) were recorded in aluminum sample holders with a laser power of 300 mW and a resolution of 2 cm^{-1}. Temperature conditions were adjusted with a SPECAC (Graesbury Specac Limited, Orpington, U.K.) variable temperature cell and a temperature control unit. The cell was evacuated (200 mbar). For investigating H_2O/D_2O exchange, the number of scans and laser power were increased to 1064 and 400 mW, respectively. Samples were stored and measured in hygrostats as detailed in ref 66 and Section 9 of the Supporting Information.

Principle component analysis (PCA), a multivariate data treatment to reduce the number of variables and provide a representation of the spectra in low dimensional space,[67−69] was used to interpret changes in the Raman spectra during dehydration. Spectra were preprocessed using min−max normalization (Opus version 5.5, Bruker Optics, Ettlingen, Germany) and first derivatives were calculated using Simca-P (Version 11.0, Umetrics AB, Umea, Sweden). The spectral region of 1800 to 30 cm^{-1} was used for constructing the PCA models.

Infrared spectroscopy was used to characterize the ionization state of the crystalline and amorphous DB7 forms (see Section 1 of the Supporting Information).

Cross-polarization/magic angle spinning NMR spectra were obtained on a Bruker Avance III 400 wide-bore NMR spectrometer operating at ^1H and ^{13}C frequencies of 400.131 and 100.623 MHz, respectively, and using Bruker 4 mm probes. The MAS rate was set to 10 kHz ± 2 Hz using a Bruker MAS-II controller. ^1H decoupling was achieved using the SPINAL64[70] decoupling sequence at a proton nutation frequency of 100 kHz. Spinning sidebands were suppressed using a five-pulse total sideband suppression (TOSS) sequence.[71] A 3.4 ms linear RF power ramp was used for cross-polarization from ^1H to ^{13}C.[72] The acquisition time was set to 34 ms, and spectra were acquired over a spectral width of 30 kHz with a recycle delay of 7 s. The ^{13}C chemical shifts were externally referenced (±0.05 ppm) to the proton-decoupled ^{13}C peak of neat (liquid) tetramethylsilane via the high-field resonance of adamantane (δ = 29.5 ppm). The sample temperature was regulated to 25 °C in order to minimize frictional heating caused by sample spinning.

2.7. Determination of Solubility.

The Crystal16 crystallization system (Avantium, NL) was used to determine the kinetic solubilities of Forms I, II°, HyA, and Hy2 in an acetonitrile/water (1:1) mixture. The temperature at the point the suspension becomes a clear solution upon heating or "clear point" (at 0.1 °C per minute, with the exception of Form I where a heating rate of 0.3 °C per minute was used to avoid transformation to Form II°) was taken as the saturation temperature of the measured sample with known concentration. To make sure that solvent-mediated transformations had not occurred during the measurements, excess solid was stirred under the same conditions, and XRPD patterns of the residual solid were recorded after reaching the highest clear point temperature derived from the solubility experiments.

2.8. Computer Model for Relative Energies and SSNMR Chemical Shift Predictions.

Periodic electronic structure calculations were carried out with the CASTEP plane wave code[73] using the Perdew−Burke−Ernzerhof (PBE) generalized gradient approximation (GGA) exchange-correlation density functional[74] and ultrasoft pseudopotentials,[75] with the addition of a semiempirical dispersion correction, either the Tkatchenko and Scheffler (TS) model[76] or Grimme06 (G06).[77] For further details see Section 11 of the Supporting Information. Energy difference estimates between the zwitterionic and neutral forms are not given because the PBE functional has been shown to overstabilize the proton transfer phases of ammonia monohydrate;[78] this systematic error should largely cancel when comparing structures with the same ionization state, as should the known limitations in modeling water−water interactions.[79,80]

NMR shielding calculations were performed on PBE-TS optimized structural models of DB7^z HyA using the CASTEP NMR code and on the fly pseudopotentials.[81] The CASTEP computed shielding constants, σ_{calc}, were converted to chemical shifts, δ_{calc}, according to $\delta_{calc} = \sigma_{ref} - \sigma_{calc}$ using a reference value, σ_{ref} taken from the zero intercepts of the fits of the calculated shielding vs. experimental chemical shift plot ($\sigma_{Castep} = -x\delta_{exp} + \sigma_{ref}$) for HyA (Section 17 of the Supporting Information).

3. RESULTS

3.1. Crystallization of Hy2 and HyA.

Our ability to meaningfully study the structures, stability relationships, and interconversion pathways of the DB7^z hydrates at a molecular level relied on securing highly crystalline, phase pure samples of each form through exquisite control over crystallization, filtration, and drying. Since both Hy2 and HyA are metastable with respect to some or all of the neat polymorphs depending on the RH, they needed to be crystallized under carefully controlled conditions, then isolated and characterized before subsequent conversion to the more stable neat forms. Selecting for the metastable hydrates in crystallization required that

amorphous DB7 be used as the starting material to ensure that the solutions were supersaturated with respect to the hydrates and free of crystalline seeds of the neat polymorphs. Even then, the filtration and drying of these materials was surprisingly tricky, with under or over drying leading to form conversions, amorphization, particle agglomeration, and mostly brittle, chunky solids. Eventually, conditions were identified to selectively crystallize and recover the hydrates in highly crystalline form, each with reasonably good material handling properties. The Hy2 and HyA materials used to fund our experimental effort were generally composed of well-formed crystals of similar size and shape commensurate with their high degree of crystallinity, phase purity, and homogeneity (Figure 2).
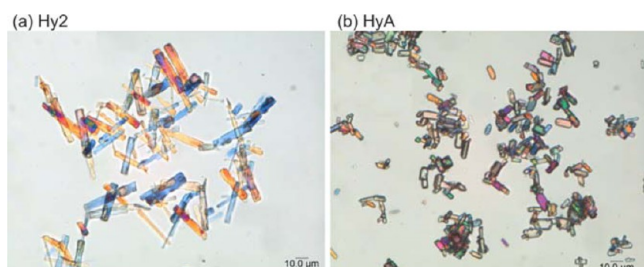
Figure 2. Photomicrographs of Hy2 (left) and HyA (right) crystals.

3.2. Single Crystal Structures and Computational Models of DB7^z Hydrates. *3.2.1. Dihydrate (Hy2).* DB7^z

Hy2 crystallizes in the monoclinic $P2_1/c$ space group with Z′=1. The molecular conformation in this zwitterionic form is closely related to one of the Form III conformers (Figure S2 of the Supporting Information), but with the carboxylic acid proton moved to the piperazine N3. Thus, the protonated piperazine is intramolecularly hydrogen bonded to the carboxylate ion (N$^+$−H···O$^-$). The DB7^z molecules form centrosymmetric dimers (Figure 3a), which are arranged in layers parallel to the *bc* plane. Each of the two water molecules (W1 and W2) forms an O−H···O hydrogen bond to one of the DB7^z carboxylate

oxygens (Figure 4); the other water protons are disordered over two positions each with a site occupancy of 0.5. W1 and
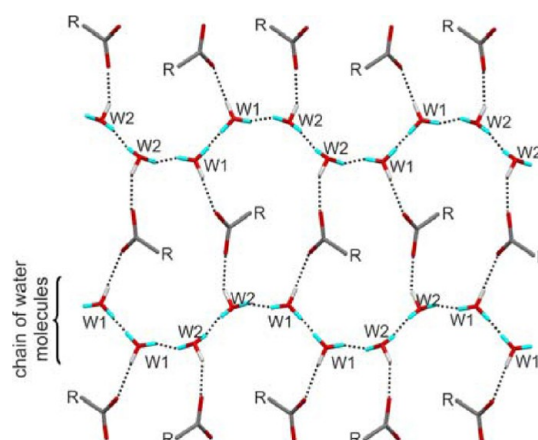

Figure 4. Hydrogen bonded sheet motif observed in Hy2. Disordered water proton positions are indicated in turquoise. View perpendicular to *bc* plane.

W2 form infinite corrugated chains, which are interlinked by the carboxylate group of DB7^z (Figure 4), leading to zigzag sheets (Figure 3b). The zigzag sheets, containing all of the strong hydrogen bonds, are interleaved in a zip motif along *a*.

3.2.2. Hydrate A (HyA). The HyA structure was determined twice using a fresh and an aged crystal. DB7^z HyA crystallizes in the monoclinic $C2/c$ space group with Z′ = 1. The main difference in the molecular conformation of DB7^z in HyA and Hy2 is a ~52° rotation of the C18−C19−C20−O2 dihedral (Figure 5a) moving the carboxylate group from an intra- to intermolecular hydrogen bonding conformation. The conformation of DB7^z in HyA is closely related to that in anhydrate Form II° (Figure S2 of the Supporting Information). Owing to the shape complementarity of the DB7^z conformers in both hydrates, inversion related dimers similar to those formed in Hy2 are also seen in HyA (Figures 3a and 5c). However, the
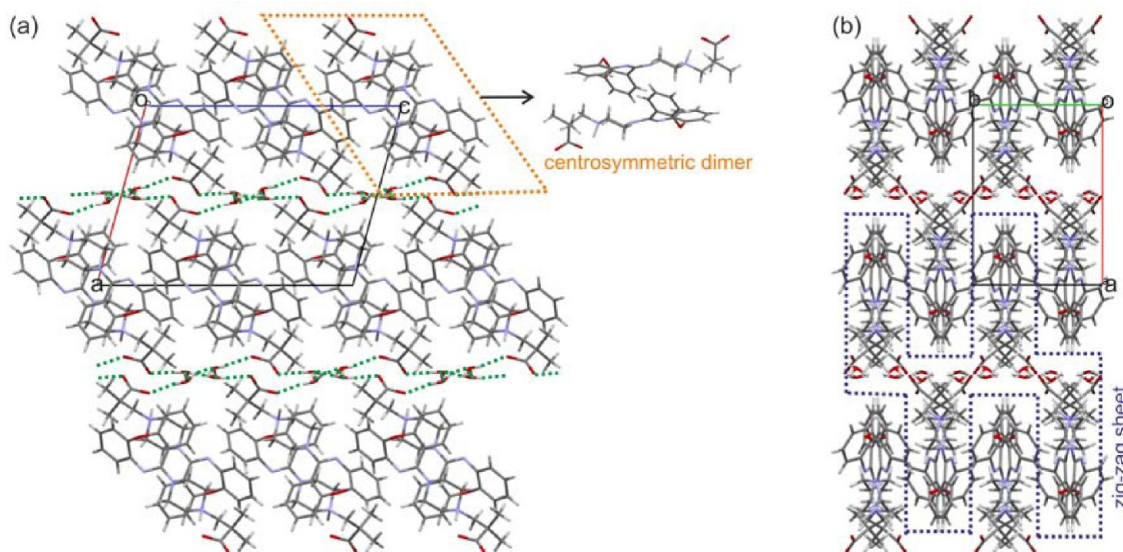

Figure 3. Packing diagram of Hy2 viewed along the crystallographic *b* axis (a) and *c* axis (b). Hydrogen bonds are denoted as green dotted lines and the centrosymmetric DB7^z dimer and zigzag sheet are highlighted.
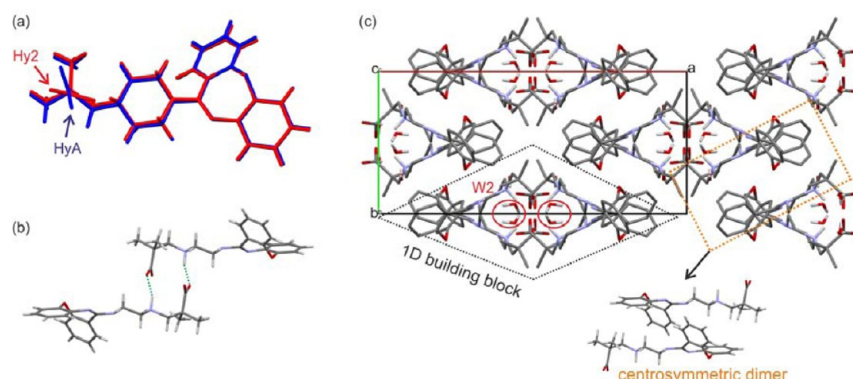
Figure 5. (a) Overlay of $DB7^z$ Hy2 (red) and $HyA_{1.95}$ (blue) conformations ($rmsd_1 = 0.38$ Å). (b) $R_2^2(12)$ dimer motif in HyA. (c) Packing diagram of $HyA_{1.95}$ viewed along c. Centrosymmetric dimer, water position W2, and 1D building block are highlighted; W1 and W3 are obscured by the carboxylate groups in this view.
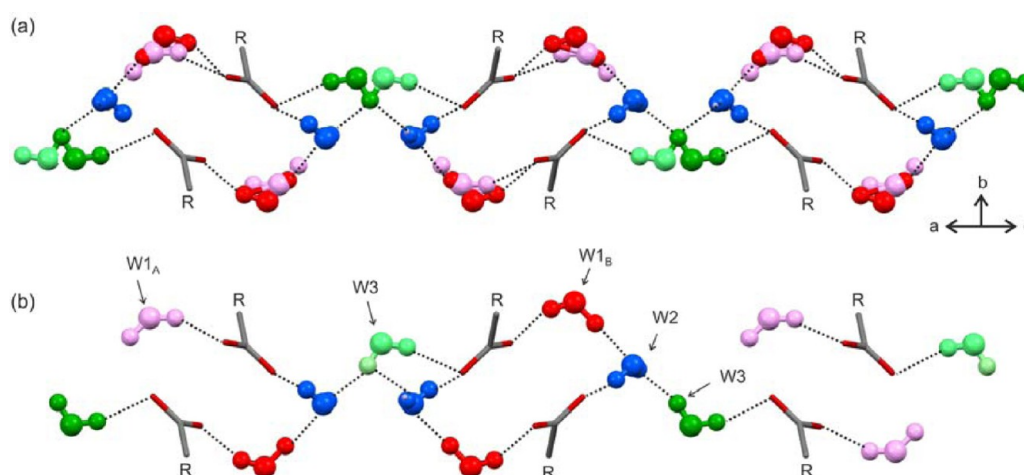

Figure 6. HyA hydrogen bonded motifs involving the water molecules and COO^- groups. The distinct water sites are coded in different colors: $W1_A$, rose; $W1_B$, red; W2, blue; W3, green. Note that only one of the two differently colored W3 orientations can be occupied as the two positions are related by a 2-fold axis at a proton position. (a) Showing the time-averaged water occupancy and (b) one of many possible instantaneous snapshots of the water positions in HyA in the range of occupancies seen in the two crystals.

HyA structure also features intermolecularly hydrogen bonded $R_2^2(12)$ dimers[82] involving strong $N^+–H\cdots O^-$ hydrogen bonds (Figure 5b).

The HyA structures of the fresh and aged crystals differ in containing 1.95 ($HyA_{1.95}$) and 1.73 ($HyA_{1.73}$) mol of water per mol of $DB7^z$, respectively. The loss of 0.22 mol of water on aging resulted in a volume change of −3.5%, with the c-axis change of −2.5% being the most significant. Three water sites (W1−3) were identified in HyA. Water site W1 is disordered over two positions, which are so close in proximity that only one of the two positions can be occupied at any time (Figure 6a). The W1 sites refined to an occupancy of 46% ($W1_A$) and 52% ($W1_B$) for $HyA_{1.95}$, and 68% ($W1_A$) and 30% ($W1_B$) for $HyA_{1.73}$. The site occupancy from the refinement of W2 was similar to that of $W1_B$, i.e., 52% for $HyA_{1.95}$ and 30% for $HyA_{1.73}$. Thus, if W2 is present, $W1_B$ is occupied, and if not, $W1_A$ is likely to be occupied (Figure 6b). Water site W3 is also disordered over two positions, which are too close to be occupied at any one time. In HyA, one of the W3 water protons is located on a special position, a 2-fold axis, so a maximum of 0.5 mol water per mol DB7 would be present at full occupancy. Refinement of the W3 waters revealed nearly full occupancy, 45% for both $HyA_{1.95}$ and $HyA_{1.73}$, across the symmetry related sites.

As in Hy2, the HyA water molecules form strong hydrogen bonds to $DB7^z$ and one another. $W1_B$ can form two $O_{W1}–H\cdots O$ interactions, involving carboxylate O1 and the W2 oxygen (Figure 6). W2 participates in four hydrogen bonds, as a donor to the carboxylate O2 and the oxepine N and an acceptor to $W1_B$ and W3. Together with the $DB7^z$ carboxylate oxygens, $W1_B$ and W2 form an extended ring motif (Figure 6). The third water molecule, W3, is hydrogen bonded to carboxylate O2 and W2 (when present), linking the hydrogen bonded rings along the c axis, the axis most affected in length by the HyA water content. The 1D hydrogen bonding network of HyA is a marked contrast to the 2D sheets of water and $DB7^z$ molecules found in Hy2. In HyA the 1D hydrogen bonded chains (Figure 5c) are close packed in the second and third dimensions through centrosymmetric $DB7^z$ dimers.

Both hydrates are zwitterionic, but the $N3–H^+$ in each structure is close to one of the carboxylate oxygen atoms. Computationally, we can confirm the zwitterionic assignment by a method used to distinguish between salts and cocrystals.[83,84] Hypothetical neutral hydrates are constructed from $cHy2$ (Section 3.4.2) and $cHyA_{2.0}$ (Section 3.4.3) by moving the acidic proton to the nearby carboxylate oxygen and adjusting the bond lengths to give a cis-carboxylic acid for HyA and the less common $trans$-acid conformation for Hy2. Full
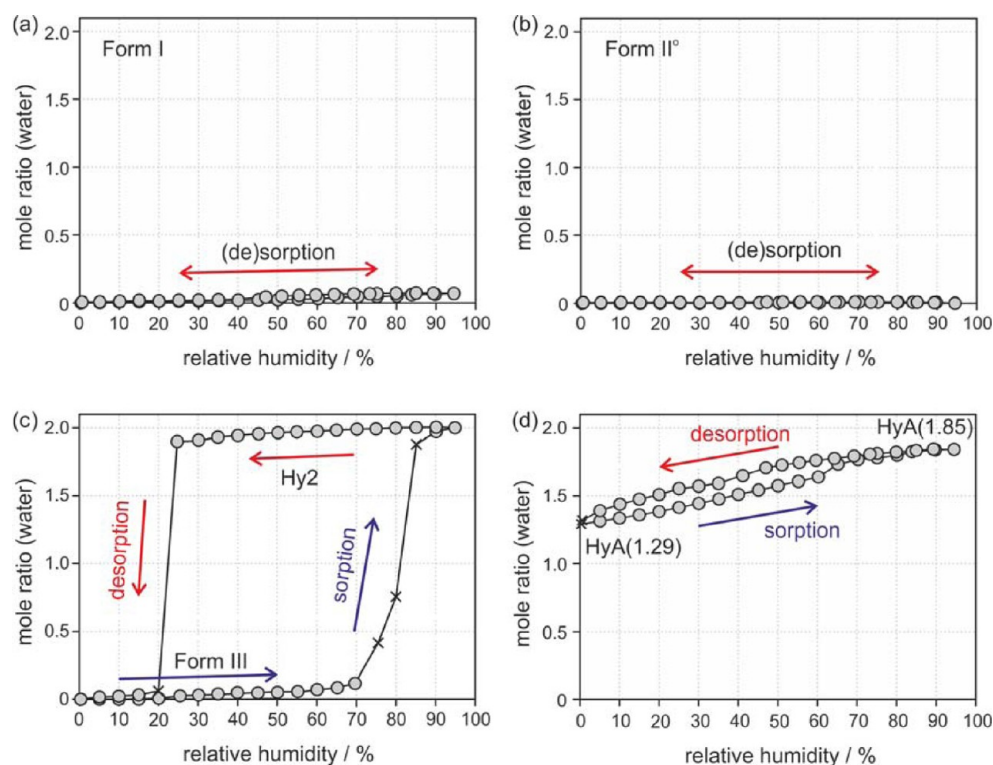
Figure 7. Gravimetric moisture sorption and desorption curves of DB7^z solid forms at 25 °C: (a) Form I, (b) Form II°, (c) Form III/Hy2, and (d) HyA. The gray circles represent data points that fulfill the preset equilibrium conditions (see Experimental Section), whereas the crosses mark measurement values that did not reach equilibrium within the allowed time limit (48 h).
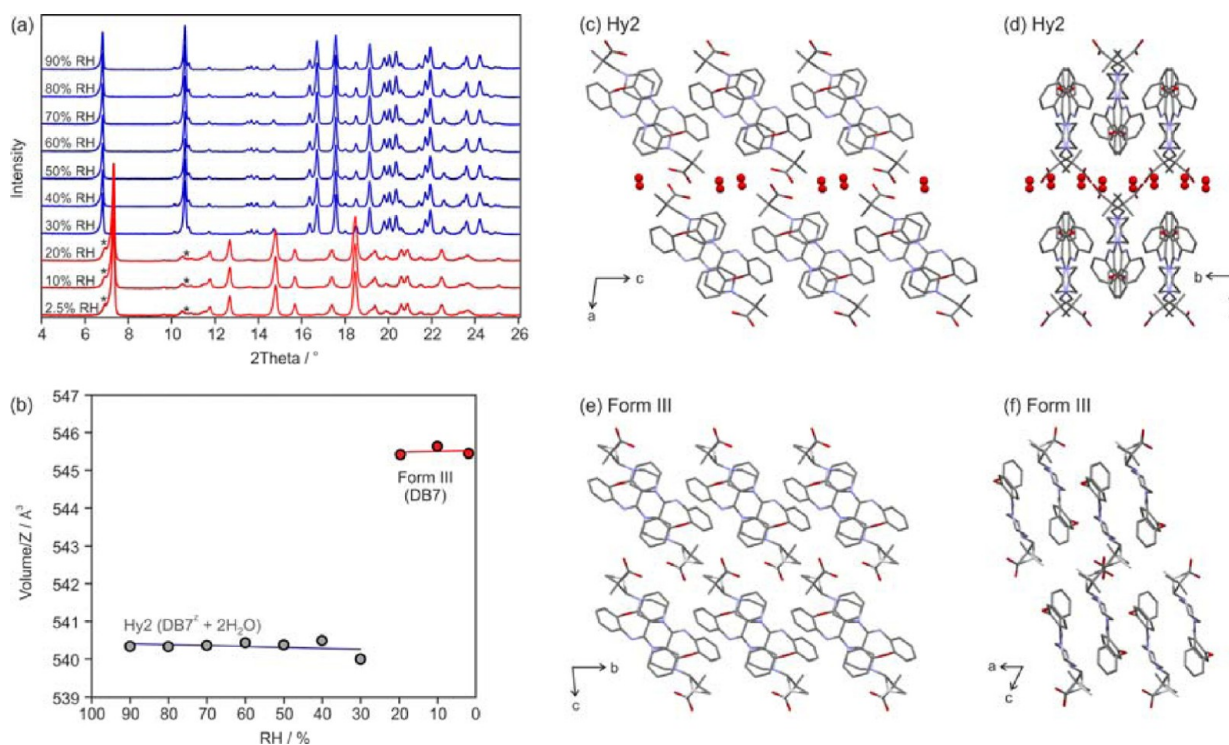

Figure 8. (a) Moisture-dependent XRPD measurements showing the dehydration of Hy2 to Form III. Peak positions marked with * correspond to Hy2 impurities (dehydration not complete due to the shorter time intervals of 12 h and 10% RH steps in contrast to ~48 h and 5% steps in Figure 7c). (b) Moisture-dependent changes in the cell volume per asymmetric unit for the transformation Hy2 to Form III. (c,d) Molecular packing of DB7^z in Hy2 and (e,f) DB7 in Form III. Water molecules are depicted as balls and hydrogen atoms are omitted for clarity. Disorder of the methyl group in Form III is indicated with different shades of gray.
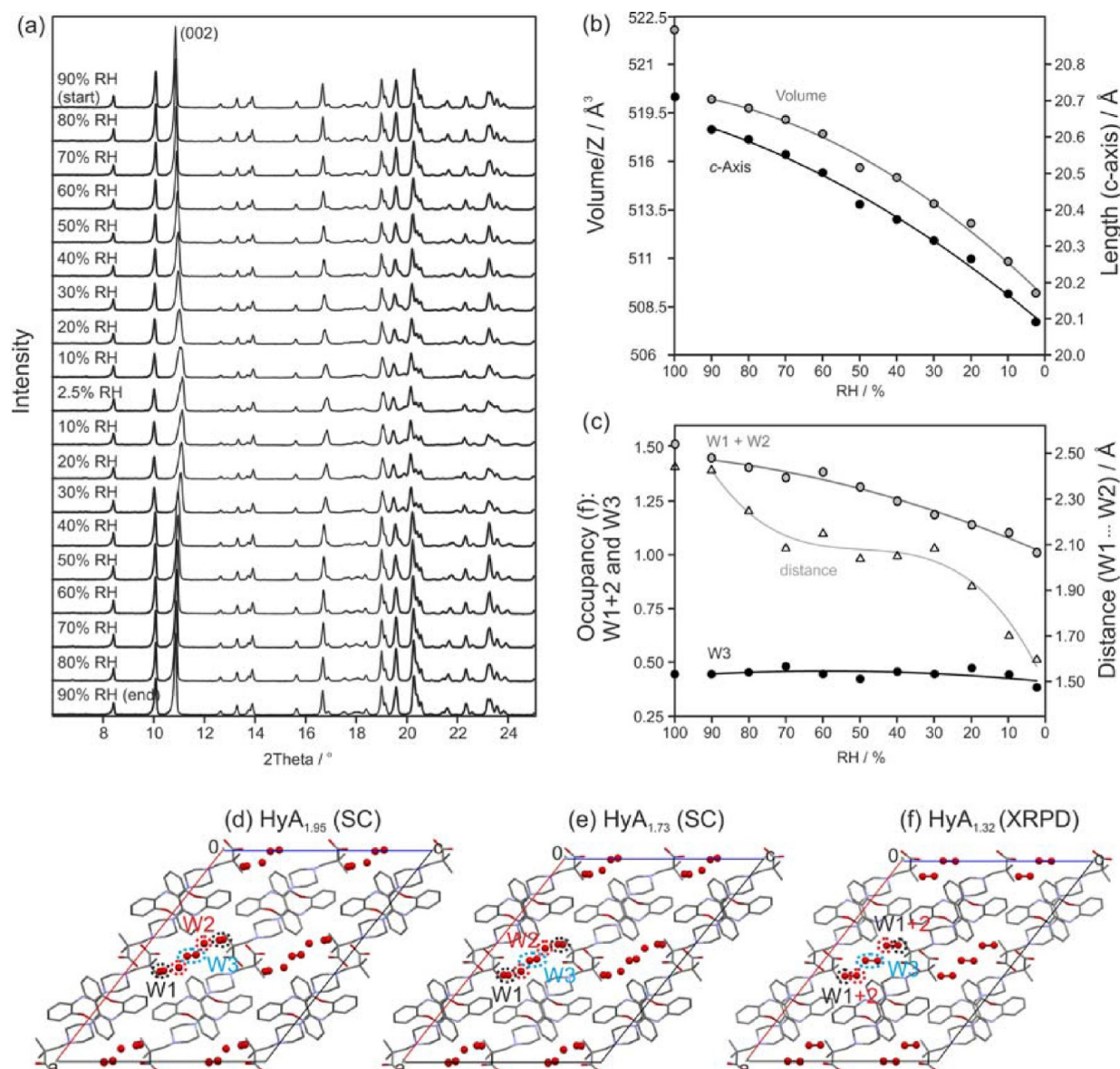
Figure 9. (a) Moisture-dependent XRPD measurements of HyA. (b,c) Changes in the HyA cell volume, length of the *c*-axis, fractional occupancies of W1 + W2 and W3 oxygens, and distance between W1 and W2 oxygens on lowering the RH (desorption). Water position W1 was modeled as one site only. 100% RH data points given in (b) and (c) were derived from slurry experiments in water. (d−f) Packing diagrams of HyA highlighting the water oxygen positions at different HyA hydration states derived from single crystal X-ray data (d,e) and Rietveld refinement of powder X-ray data (f). The dotted encirclements indicate the water positions W1−W3. Red lines between water oxygens indicate the disordered sites for W3 and close proximity of the W1 and W2 positions in (f). $W1_A$ and $W1_B$ disorder was not modeled in (f).

optimization of both charge neutral structures results in the acidic proton moving back to reform the observed zwitterionic hydrate structures, showing that both hydrates are more stable in zwitterionic than neutral form with no appreciable barrier to proton migration (Tables S5 and S7 of the Supporting Information). The converse was also found: full optimization of the corresponding hypothetical zwitterionic versions of Forms I−III results in the proton moving to give the observed locally neutral structures.[47]

3.3. Stoichiometric and Nonstoichiometric (De)-Hydration of DB7^z Hydrates. The hydration and dehydration behavior of the DB7^z crystal forms was investigated between 0% and 95% RH at 25 °C (Figure 7). Two of the anhydrates, Forms I (Figure 7a) and II° (Figure 7b), show almost no water uptake (Form I < 0.32% and Form II° <

0.04%) up to 95% RH. In contrast, anhydrate Form III undergoes a phase transformation with a mass increase corresponding to 2 mol of water per mol of DB7 at RH values >70% (Figure 7c). The product hydrate phase, confirmed to be Hy2 by XRPD, shows good RH stability with a marginal weight loss between 95 and 25% RH. Below 25% RH, dehydration is rapid. Hysteresis was observed in the Form III/Hy2 isotherm despite the lengthy equilibration times (up to 48 h) at each RH. The profile of the moisture sorption/desorption isotherms for Form III ↔ Hy2 with steps accompanied by phase changes, is typical of a stoichiometric hydrate.[3] In contrast, highly crystalline HyA shows the typical (de)sorption isotherms of a nonstoichiometric hydrate[3] (Figure 7d, see also Figure S3 of the Supporting Information) as the mass gradually changes depending on the humidity during sorption and desorption.

3076

The lowest water content measured by TGA (Figure 7d) for HyA equilibrated at 0% RH corresponded to 1.29 mol of water per mol of DB7^z. The maximum water vapor uptake into the HyA structure was estimated to be approximately 1.85 mol of water per mol of DB7^z at 95% RH.

The automated gravimetric moisture sorption/desorption analysis of Hy2 and HyA was complemented with long-term drying experiments at 0% RH (storage over P_2O_5). Dehydration of Hy2 was observed immediately at this condition, and Form III was determined to be a kinetic dehydration product, with further transformation to the more stable Forms I and II° occurring within 2 weeks. HyA could be similarly dehydrated at 0% RH; however, loss of the last strongly bound ~1.3 waters of crystallization from this hydrate leads to a structural collapse to mainly amorphous DB7. The amorphous form has limited stability at 0% RH as there was evidence of Forms I and II° nucleating in small amounts during the low RH drying.

3.4. Structural Insights into the Hy2 and HyA Dehydration. *3.4.1. Moisture-Dependent XRPD Studies.* The gravimetric moisture sorption/desorption studies (Figure 7) were correlated with structural changes to Hy2 and HyA using variable-humidity XRPD at 30 °C (Figures 8 and 9). In agreement with the results obtained in Figure 7c, distinct changes occur in the XRPD pattern of the Hy2 sample at RH values <30% (Figure 7a). The disappearance of high intensity Hy2 peaks (e.g., at 6.82, 10.62, 16.37, 16.71, and 17.57° 2θ) and appearance of Form III peaks (e.g., 7.33, 12.68, and 14.81° 2θ) indicate a major change in the crystal structure (Figure 8c–f) on loss of the waters of crystallization. The unusual increase in volume/Z upon dehydration (Figure 8b) can be attributed to the less efficient packing of DB7 with itself and the disorder observed in Form III.

In contrast to Hy2, there is no significant change in the crystal lattice of HyA with varying RH (Figure 9b) apart from anisotropic expansion of the network to accommodate a variable amount of water. The anisotropy of the lattice expansion was quantified by indexation and Rietveld refinement of the HyA XRPD patterns recorded at different RH values (Figure 9a). Using the HyA$_{1.95}$ structure as a starting model, Rietveld refinement found the c axis to be affected the most by changes in the water content, in agreement with the SCXRD experiments, but over a wider range of compositions (Table S2 of the Supporting Information). Structural refinement also revealed that the water occupancy of W3 stays close to 50% (i.e., full) independent of the RH, suggesting that the W3 position is integral to the HyA structure. However, the occupancy parameters for W1 and W2 collectively decreased at progressively lower RH values. The W1···W2 distance was also found to depend on the hydration state. At moderate RHs (20–80%) a plateau is reached with the modeled W1···W2 distance being too short for two distinct sites, suggesting either water mobility or static disorder (Figure 9c). A further distinct change in the W1···W2 distance is seen below 25% RH, the moisture range where in addition to continued diffraction peak shifting, selected reflections, in particular (002), are broadened. Peak broadening provides yet another indication of structural disorder. The lowest HyA water content observed in the RH-dependent XRPD experiments of HyA was 1.32 mol of water per mol of DB7^z (measured with TGA).

The moisture-dependent XRPD experiments were extended to water activity = 1 (~100% RH)[85] by measuring a thick HyA slurry in water. The powder pattern of the 100% RH HyA sample refined to 1.96 mol equiv of water per DB7^z, comparable to HyA$_{1.95}$ observed (by SCXRD) for a freshly crystallized single crystal. While a change in water content and unit cell volume was to be expected on increasing the RH from 90 to 100%, the sharp uptake of 0.10 mol water per mol DB7^z and unit cell volume increase of 0.5% (Figure 9b) was unexpected and presumably reflects the slow hydration kinetics of HyA in the solid state (Table S2 of the Supporting Information).

3.4.2. Lattice Energy and Dehydration Modeling of Hy2. An ordered Hy2 structural model was derived from the experimental crystal structure by replacing the two disordered water molecules related by a 2_1 screw axis with one molecule in each orientation (Section 12 of the Supporting Information). This lower symmetry Hy2 structure (Figure S10b) was lattice energy minimized to give the computational model of the Hy2 structure, denoted cHy2.[86,87]

The geometry optimizations of four hypothetical hydrate and framework structures derived from cHy2 (Table S5 of the Supporting Information) showed that proton transfer to a neutral DB7 molecule occurred when there was no water hydrogen bonding to the carboxylate oxygen involved in the N$^+$−H···O$^-$, suggesting that W2 stabilizes the zwitterionic form of Hy2. Although the layer structure (Figure 2) suggests that it might be possible to remove both W1 and W2, doing this computationally results in proton transfer and an unstable, low density isomorphic desolvate[88] with no strong hydrogen bonds between DB7 molecules. Partial removal of the W1 molecule gave hypothetical zwitterionic sesquihydrate (cHy2$_{1.5(0.5W1+W2)}$) and monohydrate (cHy2$_{1.0(W2)}$) structures, which differed in lattice energy from Hy2 by 55 and 107 kJ mol^{-1}, respectively (Table S5 of the Supporting Information, averaged over the two dispersion models). Estimating whether Hy2 could undergo a phase transition to an isostructural sesqui- or monohydrate requires comparison of the lattice energies of the model hydrates with that of ice (Section 16 of the Supporting Information). This gives an unfavorable phase transition energy of more than 30 kJ mol^{-1} for each water removed. Thus, the computational thermodynamic estimates show that a stepwise dehydration of the Hy2 structure, preserving the Hy2 DB7^z framework structure (i.e., a structurally related sesquihydrate or monohydrate as a transient, intermediate hydrate along the dehydration pathway), is highly unlikely. This is consistent with Hy2 showing a single stepwise weight loss by moisture sorption analysis (Figure 7c) and TGA (Section 3.5.1) to water free DB7.

3.4.3. Lattice Energy and Dehydration Modeling of HyA. The two HyA structures show a similar nearly full occupancy of W1$_A$ + W1$_B$ (98%) and W3 (45%), but differ in the W2 partial occupancy (52% or 30%). To form an ordered computational model of HyA$_{1.95}$, the crystallographic 1.95 water molecules per DB7^z molecule had to be increased to 2 by modeling the 98% (46% W1$_A$ + 52% W1$_B$), 52% and 45% occupancy ratios for W1, W2, and W3 as 100%, 50%, and 50%, respectively. All symmetry was removed from the C2/c, Z′ = 1 structure of HyA, resulting in a P1, Z′ = 4 cell in which the four W1 sites are independently occupied and half of the W2 and W3 sites are occupied (Section 13 of the Supporting Information). All possibilities leading to the described occupancy ratios were used as starting structures and the lowest energy structure after geometry optimization was used as cHyA$_{2.0}$ hereafter. Similarly, for the HyA$_{1.73}$ structure the occupancies were modeled as 100%, 25%, and 50% for W1, W2, and W3 giving a model
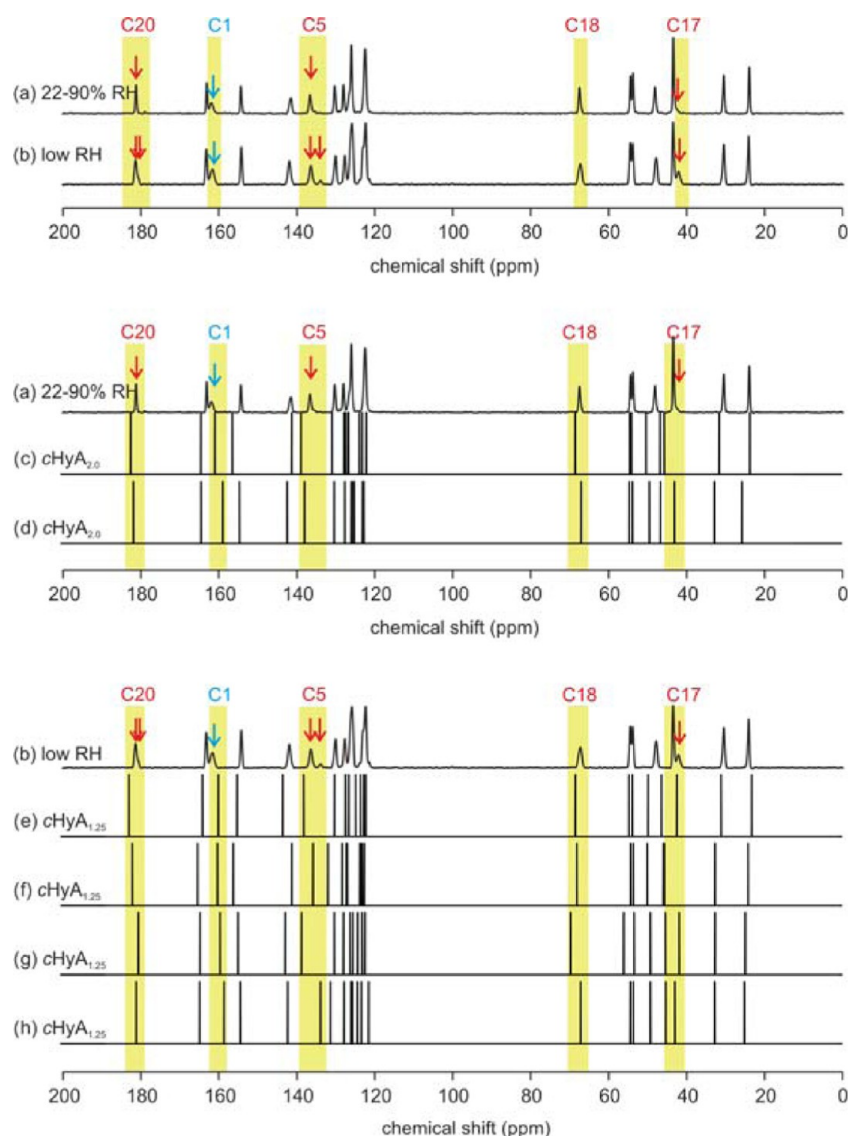
Figure 10. (a,b) Representative experimental HyA spectra differing in water content and (c−h) six of 80 NMR-CASTEP computed ^{13}C CP/MAS NMR spectra. (c,d) The two DB7^z environments observed in the ordered *P1 c*HyA$_{2.0}$ model and (e−h) the four environments observed in the ordered *P1 c*HyA$_{1.25(13)}$ model, which correspond to 0.75 W1, 0.25 W2, and 0.25 W3.

*c*HyA$_{1.75(2)}$ (Table S7 of the Supporting Information), which agreed with the experimental structure. The confirmation that the ordered cell models *c*HyA$_{2.0}$ and *c*HyA$_{1.75}$ were reasonable representations of the disordered structures is given in Section 15 of the Supporting Information.

A set of hypothetical HyA framework structures can be derived from the experimental structure, ranging from a hemipentahydrate (*c*HyA$_{2.5}$, 2.5 mol of water per mol DB7 at full W1 and W2 occupancy) to the water free framework (Table S7 of the Supporting Information). The lattice energy of *c*HyA$_{2.5}$ was higher (less stable) by about 2 kJ mol^{-1} than the sum of the lattice energies of *c*HyA$_{2.0}$ and 0.5 mol of ice XI,[89] implying that additional water to fully occupy the W2 site would destabilize the HyA structure. This rationalizes[54] why the fully hydrated hemipentahydrate stoichiometry is not observed experimentally.

Computational dehydration of *c*HyA$_{2.0}$ to *c*HyA$_{1.75}$, *c*HyA$_{1.5}$, and *c*HyA$_{1.25}$ produces a range of possible structures, which are very close in energy (Table S7 of the Supporting Information). Removal of water from HyA was calculated to be energetically

quite feasible and to require considerably less energy than removing comparable amounts of water from Hy2 (Tables S5 and S7). Overall, each of the water sites adjusts to optimize Ow−H⋯O$^-$ (carboxylate) hydrogen bonding upon structure optimization.

The calculated isomorphic HyA desolvate (*c*HyA$_{0.0}$) also undergoes a proton transfer to the neutral molecule on optimization (Table S7 of the Supporting Information). In fact, proton transfer from DB7^z to DB7 was observed when the carboxylate of the N$^+$−H⋯O$^-$ $R_2^2(12)$ dimer (Figure 5b) was not also acting as an acceptor for an Ow−H⋯O$^-$ hydrogen bond. Thus, the hydrogen bonded water molecules (W1, W2, or W3) appear to be essential for zwitterion formation. Since *c*HyA$_{0.0}$ is estimated to be over 25 kJ mol^{-1} less stable than Form II°, an isomorphic desolvate of HyA containing zwitterionic or neutral DB7 molecules is unlikely to form. This is consistent with a destructive dehydration mechanism on loss of all waters of crystallization.

3.4.4. Moisture-Dependent SSNMR Spectroscopy and Chemical Shift Calculations. The suggestion of water
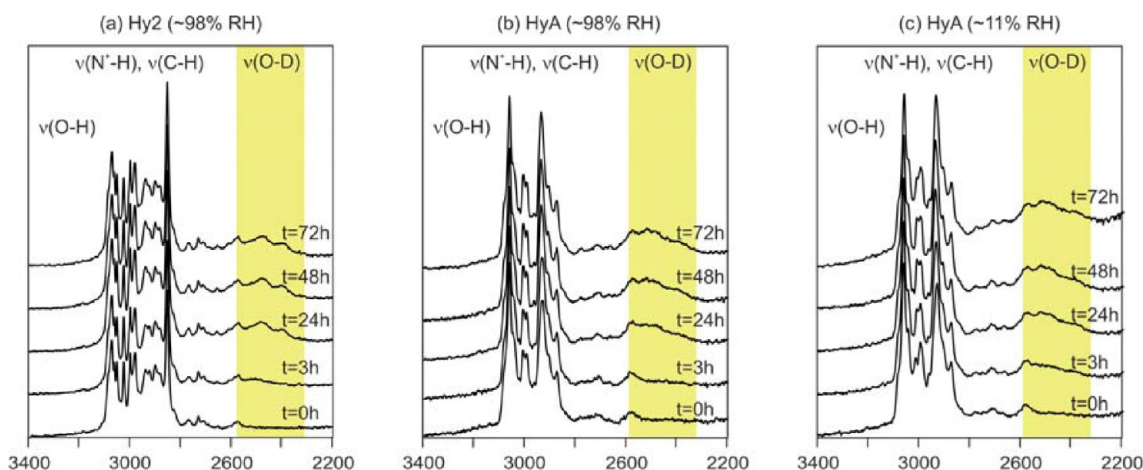
Figure 11. Raman spectra of DB7^z Hy2 (a) and HyA (b,c) as a function of time of exposure to D$_2$O vapor, ~98% RH (a,b) and ~11% RH (c). Peaks due to O−D stretching vibrations emerge over the course of 72 h.

mobility/disorder from the diffraction experiments and static lattice energy modeling led to the use of ^{13}C CP/MAS NMR spectroscopy[90] to characterize HyA as a function of water content. Except for slight peak intensity variations, the SSNMR spectra of HyA samples equilibrated between 22 and 90% RH were essentially identical (Figure 10a; Figure S5 of the Supporting Information). Since partial occupancy of the HyA water sites over this RH range would necessarily result in a distribution of hydrogen bonding arrangements (Figure 6), the observation of a single ^{13}C resonance for each carbon atom in DB7^z shows that the different hydrogen bonding environments are effectively "averaged" as the waters of crystallization move in and out of the water sites in the HyA crystal structure. Thus, SSNMR shows that the water of crystallization is highly mobile over a wide range of moderate and high RH.

After equilibrating the sample at RH ≤ 11% (Figure 10b), peak splitting for carbon atoms C20, C5, and C17 and broadening of several ^{13}C NMR resonances were seen across the SSNMR spectrum of HyA. The additional peaks were not due to Forms I−III[47] or Hy2 (ref 47 and Figure S6 of the Supporting Information) phase impurities, as there is no match to their chemical shifts. Instead, the emergence of low intensity peaks was ascribed to restricted water mobility in the contracted HyA cell, which would also explain the diffraction peak broadening seen in Figure 9a. Support for this interpretation of the low RH SSNMR spectrum (Figure 10) comes from DFT shielding calculations on 25 variably hydrated cHyA structures (Section 17 of the Supporting Information), which generated 80 ^{13}C NMR spectra of DB7^z in different HyA water environments. These showed that the chemical shifts of C20, C5, C18, and C17, because of their proximity to the water molecules, were particularly sensitive to hydration state and water positions, varying by 3−5 ppm (Table S11 of the Supporting Information). Since the regions in the SSNMR spectrum shown computationally to be most sensitive to water in the HyA structure coincide with those where peak splitting is observed at low RH (Figure 10), we can account for the peak splitting as a manifestation of reduced water mobility on the SSNMR time scale.

In contrast to HyA, the SSNMR spectra of Hy2 (Figure S6 of the Supporting Information) show a distinct phase change to Form III in this case between 11 and 22% RH, in good agreement with the moisture sorption (Figure 7c) and XRPD data (Figure 8a,b).

3.4.5. Water Diffusion in DB7^z Hydrates Monitored Using H/D Exchange.
Hy2 and HyA were exposed to deuterium oxide vapor (~98% and ~11% RH) and characterized by Raman spectroscopy at different time points (Figure 11) to investigate water dynamics in the two hydrates. The wavenumber region 3400−2800 cm^{-1} is composed of peaks arising from ν(O−H), ν(N$^+$−H), and ν(C−H) stretching vibrations; ν(O−D) stretching modes of D$_2$O are seen between 2600 and 2300 cm^{-1}. The emergence of O−D peaks in the spectra of both hydrates on exposure to deuterium oxide vapor confirms that D$_2$O displaces H$_2$O in both crystal structures. Thus, not only is the water of crystallization in HyA mobile, but water exchange is also observed for the stoichiometric hydrate, Hy2. Water diffusion in and out of the two crystal structures is rapid and quantitative, as derived from the fact that the Raman spectra after exposure to D$_2$O for 72 h were indistinguishable from fully deuterated Hy2 and HyA. DB7^z also has an ammonium proton that could exchange a hydrogen for a deuterium. To see whether the ammonium group had undergone exchange, the hydrate samples that had been exposed to D$_2$O vapor were dehydrated and compared to the Raman spectra of the neat forms. The comparison showed that within 72 h of D$_2$O vapor exposure the ammonium group was not affected at all.

3.5. Thermal Dehydration Reactions/Phase Transformations.
3.5.1. Hot-Stage Microscopy, Thermogravimetric Analysis, and Differential Scanning Calorimetry.
The TGA curve of Hy2 (Figure 12a) shows a one-step mass loss of 8.67 ± 0.05%, corresponding to exactly two mole equivalents of water. Dehydration starts immediately under the dry conditions of a nitrogen purge.[91] On removing the water of crystallization, the clear Hy2 crystals turn opaque, but maintain their shape ("pseudomorphosis"[92,93]).

Slow heating DSC experiments of Hy2 (Figure 12a) using pinhole lids show four events: (1) dehydration of Hy2 to Form III takes place below 45 °C. (2) At 95 °C there is an exothermic phase transformation of Form III mostly to Form II°, with minor amounts of Form I present. The measured enthalpy of transition is in agreement with the value derived using pure Form III as a starting material ($\Delta_{trs}H_{III−II}$ = −13.3 ± 0.2 kJ mol^{-1}).[47] (3) Upon further heating, melting of the minor Form I component is observed at an onset temperature of 176.0 ± 0.4 °C (small peak). (4) At an onset temperature of 180.9 ± 0.2 °C, the Form II° melts.
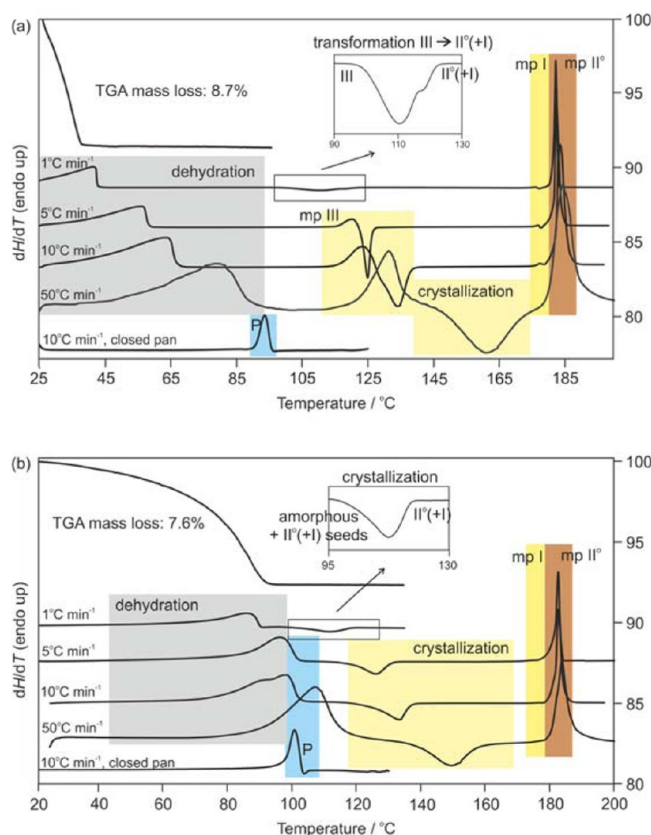
Figure 12. Differential scanning calorimetry (DSC) and thermogravimetric analysis (TGA) thermograms of (a) Hy2 and (b) HyA. TGA curves were recorded in open pans at a heating rate of 5 °C min⁻¹. Five pinhole lids were used for the DSC experiments, unless specified otherwise. Mp, melting point; P, peritectic decomposition peak.

By increasing the heating rate used in the Hy2 DSC experiments to 5 °C min⁻¹ or more (Figure 12a: 5, 10, and 50 °C min⁻¹), an additional thermal event is observed above 118 °C corresponding to the inhomogeneous melting of Form III. Melting is followed by the recrystallization of mainly Form II°, then the melting of Forms I and II°. By embedding the Hy2 crystals in high viscosity silicone oil or using hermetically sealed DSC pans (Figure 12a), the incongruent melting of Hy2 (peritectic decomposition) is observed at 89.8 ± 1.3 °C.

Compared to Hy2, higher temperatures are required to fully dehydrate HyA. By TGA, a HyA sample pre-equilibrated at 75% RH (stored over a saturated NaCl solution) showed a mass loss of $7.61 \pm 0.04\%$, corresponding to 1.74 mol equivalents of water (Figure 12b). Toward the end of the dehydration process a loss of birefringence is observed in polarized light, indicating that the strongly bound water is released by a process that leads to a loss of crystallinity. Simultaneous nucleation of a few crystals could be seen. The generation of mainly amorphous DB7 with Form I and II° impurities was independently confirmed by XRPD and Raman spectroscopy.

The loss of crystallinity upon dehydrating HyA was also supported by DSC, based on the appearance of an exothermic event immediately following the dehydration endotherm. Upon further heating, the few crystal nuclei produced at lower temperatures (during dehydration) grew into a mixture of Forms I and II°, evidenced by the final two melting events. The

lower the dehydration temperature, the less Form II° was observed.

DSC traces of HyA collected at faster heating rates ($\geq$10 °C min⁻¹) show an overlap of dehydration and peritectic decomposition at 99 °C. The peritectic decomposition of HyA, measured in hermetically sealed DSC pans, is observed at 98.9 ± 0.9 °C.

3.5.2. Temperature-Dependent Raman Spectroscopy. Raman spectra were recorded for Hy2 and HyA every 2 to 5 °C from 25 to 130 °C, then subjected to PCA to track the solid state transformations (Figure 13b,c) by comparison to reference spectra of the DB7 forms (Figure 13a). The Raman spectra recorded throughout the Hy2 dehydration appear as three distinct clusters, corresponding to Hy2, Form III, and Form II° with Form I impurities; in between the clusters (50, 100, and 102 °C, Figure 13b) are mixed phases. These results show that Form III is a distinct intermediate phase along the thermally induced dehydration pathway of Hy2. (The close proximity of the dehydration product to phase pure Form II° relative to phase pure Form I in Figure 13b shows that Form II is the main component, and the tightness of the final product cluster shows that the Form I impurities did not transform to Form II.) This dehydration pathway is in agreement with the DSC and TGA results in Figure 12a. The dehydration of Hy2 does not go via an appreciably stable amorphous phase or phase pure Form I because the triangles representing Form I and amorphous DB7 are not located on the dehydration pathway.

The structural changes accompanying the dehydration of HyA to a Form I and II° mixture could be described with three PCs, but a continuous transformation pathway is evident from two of them, Figure 13c. As the small structural variation within HyA exhibiting variable water content between 25 and 62 °C is apparent by PC2, PC1 shows the transformation from the HyA crystal lattice (70 °C) through the amorphous state (82 °C) to the Form I/II° mixture (86−130 °C) (Figure 13c).

3.5.3. Hy2 to Form III Phase Transformation. Form III was obtained for the first time following the salt disproportionation of DB7 phosphate at pH $\geq$ 6. Only after we were unable to directly crystallize Form III from solution and systematically studied the dehydration mechanism of Hy2 was it evident that Hy2 was the kinetic phosphate salt disproportionation product and necessary intermediate phase for obtaining Form III. Structural analysis has shown that the molecular conformation of DB7ᶻ in Hy2 with intramolecular hydrogen bonds seems to predispose it to dehydration to Form III, the only anhydrate, which also features intramolecular hydrogen bonding.[47] To the best of our knowledge, Form III has never nucleated directly from solution or the melt.

Following our observation of batch-to-batch variability in the disorder ratio of the dimethylpropionic acid side chain in Form III, we performed systematic drying studies of Hy2 to estimate the effects of RH and temperature on the level of disorder present in the Form III dehydration product and to seek conditions that would select for the ordered structures. The disorder ratio was quantified from the intensities of the dimethylpropionic acid methyl ¹³C SSNMR peaks (Figure 14a, Table S3 of the Supporting Information). Unfortunately, despite the wide range of drying conditions surveyed, we were not successful in preparing either an ordered Form III sample or one having the minor conformation dominating.

Subsequent DSC investigations (Figure 14b) were conducted to examine whether the disorder ratio in Form III influences its solid form transformation to Forms II° and/or I.
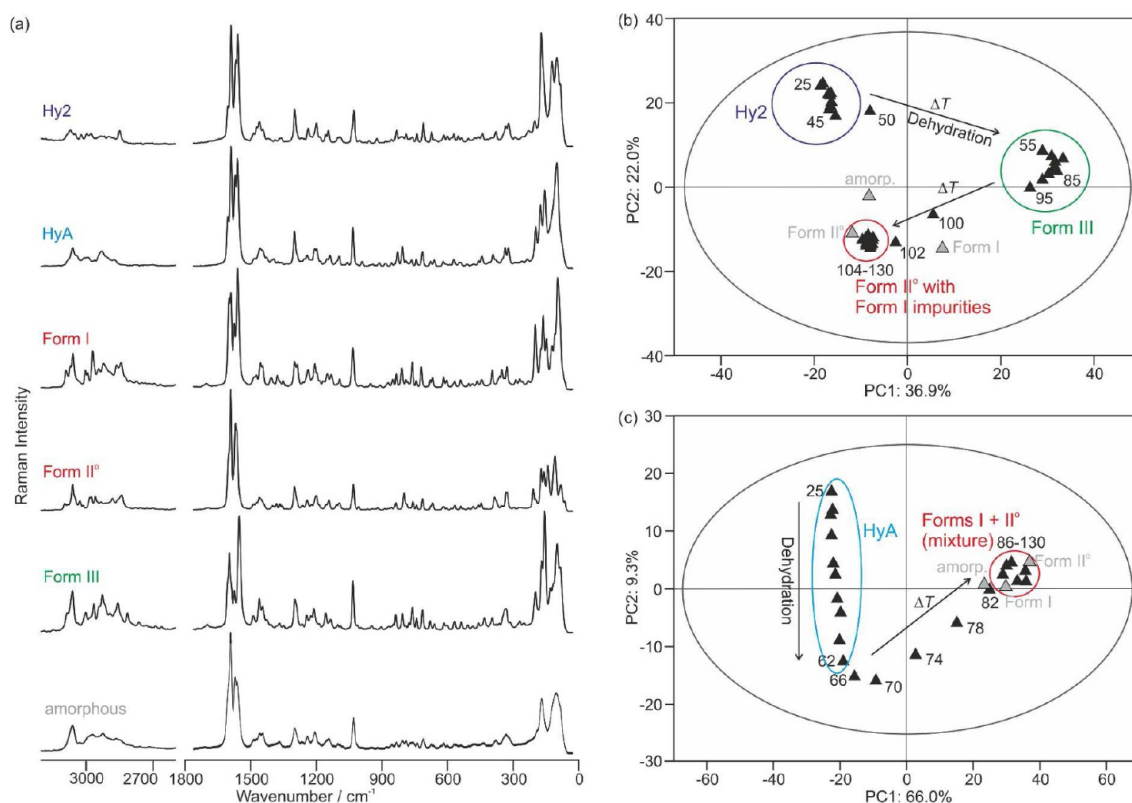
Figure 13. (a) FT-Raman spectra of DB7^z solid forms. (b,c) Raman principal component analysis (PCA) plots for the first and second principal component (PC1 and PC2) of DB7^z forms occurring during dehydration of Hy2 (b) and HyA (c). Separate models were generated for the two dehydration processes. Each triangle corresponds to a Raman spectrum: black, recorded during dehydration and used for constructing the PCA models; gray, reference spectra for Forms I and II° and amorphous DB7. Arrows highlight the reaction pathway. Numbers correspond to the temperature at which each spectrum was recorded; black ellipse corresponds to the 95% hotelling T2, and areas of distinct DB7^z solid forms are encircled. The %-values on the axes indicate the data variance modeled by the respective PC.
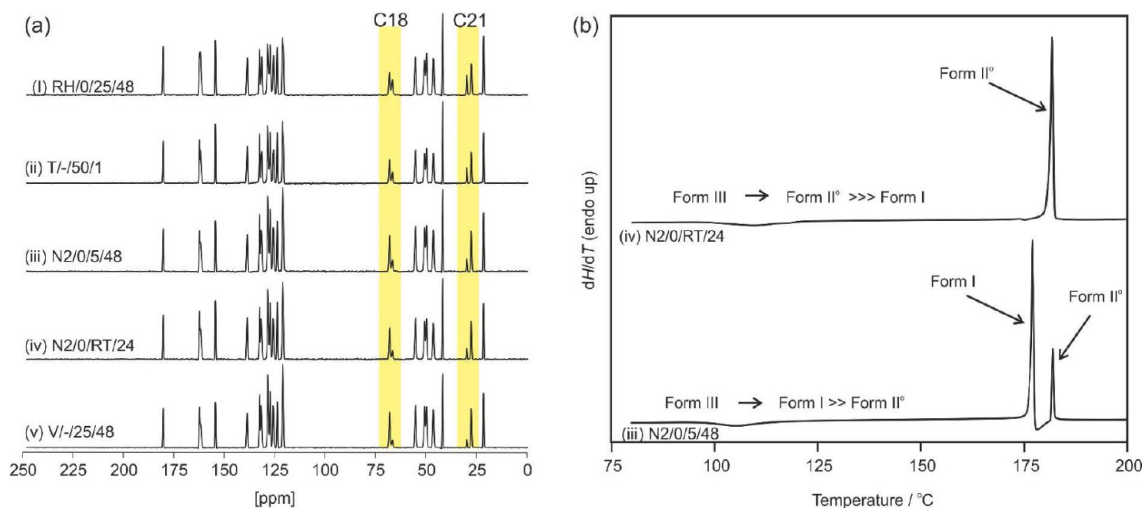

Figure 14. (a) ^{13}C CP/MAS NMR spectra of DB7 Form III produced by dehydrating Hy2 under a variety of conditions (defined in the Supporting Information, Table S3). Highlighted are the C18 and C21 peaks characterizing the structural disorder of the dimethyl propionic acid side chain. (b) DSC thermograms of DB7 Form III lots N2/0/RT/24 and N2/0/5/48 measured at a heating rate of 1 °C min^{-1}. Lot N2/0/RT/24 was prepared by drying Hy2 under N$_2$ purge at room temperature for 24 h and lot N2/0/5/48 under N$_2$ purge at 5 °C for 48 h.

Although the outcomes were somewhat variable, Form III samples obtained by drying Hy2 under a variety of conditions (Table S3 of the Supporting Information) ranged from having only small amounts of Form I to as much as 90% Form I after the solid state transformation. Importantly, the heat induced phase transformation does not seem to be related to the

disorder in Form III. Form III samples N2/0/5/48 and N2/0/RT/24, for example, show a similar level of disorder in their ^{13}C SSNMR spectra, but differ substantially in their thermal behavior (Figure 14b). Thus, while the dehydration reaction of Hy2 always produces the two different conformations in Form III, small differences in the phase purity and sample

history also influence the outcome of the solid form transformation to Forms I and/or II°.

3.6. Relative Thermodynamic Stability of Hydrate/Anhydrate Phases. *3.6.1. Temperature Stability.* The DB7[z] hydrates and DB7 anhydrates showed appreciable kinetic stability in the solid state based on the gravimetric moisture sorption/desorption analysis. However, these forms were not sufficiently stable in suspensions to obtain equilibrium solubility data of interest for quantitatively establishing their thermodynamic stability relationships. The stability order of the two stable anhydrate polymorphs Forms I and II° and the two hydrate forms was therefore qualitatively estimated as a function of temperature from kinetic solubility measurements in acetonitrile/water (1:1). This solvent mixture was chosen because the DB7 and DB7[z] solid forms were sufficiently soluble to meaningfully estimate their relative solubility using the Crystal16 parallel reactor system. Unfortunately, the fast transformation kinetics of Form III to Form II° in stirred solvent prevented any measurement of the kinetic solubility of Form III.

The acetonitrile/water solubility data for Forms I and II° (Figure 15a) agree with the monotropic relationship previously derived from solubility measurements in methyl isobutyl ketone and DSC experiments,[47] as the kinetic solubility data plotted in van't Hoff form showed no signs of convergence or crossover below the DB7 melting temperature (Figure 15b). HyA is less soluble than Hy2 in acetonitrile/water (water activity, a_w, of 1:1
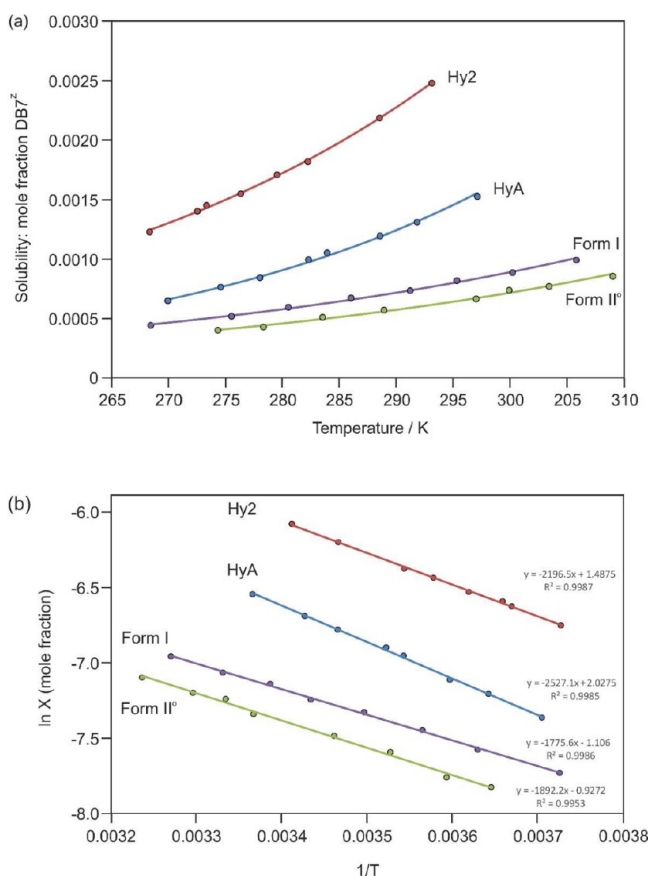
mixture is ∼0.9 at 25 °C, Figure 15a), with the van't Hoff plots further suggesting that HyA is the thermodynamically most stable DB7[z] hydrate at this water activity below the hydrates' melting points. The zwitterionic hydrates are much more soluble than the charge neutral neat forms at all measured temperatures, but their relative solubility is clearly decreasing with decreasing temperature (Figure 15b).

3.6.2. RH Stability. The critical water activity defining the crossover in thermodynamic stability of the DB7[z] hydrate−DB7 anhydrate pairs could not be determined from the solubility measurements at a single water activity; however, these results did reveal that both Forms I and II° are more stable than Hy2 and HyA at water activities up to at least 0.9 over the investigated temperature range. Above a_w = 0.9, the RT thermodynamic stability order of the DB7/DB7[z] forms was investigated through slurry experiments in methanol/water mixtures[8,94] (Section 8 of the Supporting Information). DB7[z] Hy2 and HyA were separately added to methanol/water mixtures (a_w = 0.9, 0.95, and 1.0) and stirred for 21 days. Slurries in mixtures of a_w = 0.9 and 0.95 resulted in Form II°, while the pure water slurry yielded HyA. In showing that Form II° is more stable at a_w = 0.95 and HyA is more stable in pure water (a_w = 1.0, pH 5.9), the critical water activity at which the solubility order of Form II°/HyA is reversed was more precisely bracketed between 0.95 and 1.0.

The Hy2 to HyA transformation in water did not allow us to estimate the Hy2 a_w dependency. Therefore, we used gravimetric sorption/desorption experiments to estimate the influence of moisture. The Hy2 sample used in Figure 16 was
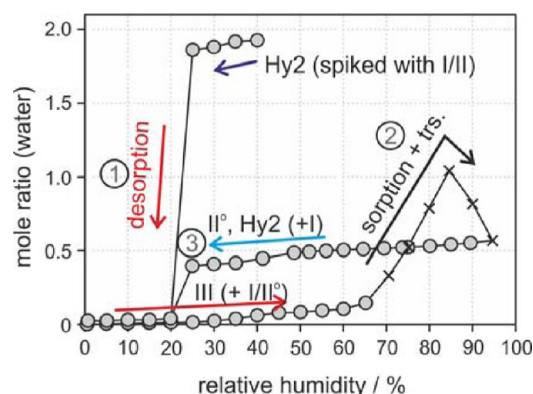

(a)

(b)

Figure 15. (a) Solubility (mole fraction) of DB7[z] Forms I, II°, Hy2, and HyA in acetonitrile/water (1:1, $a_w \approx 0.9$) as a function of temperature and (b) van't Hoff plot of the molar solubility as a function of temperature.

Figure 16. Gravimetric moisture sorption and desorption curve of DB7[z] Hy2 spiked with Forms I and II° at 25 °C. The gray circles are data points that fulfill the preset equilibrium conditions (see Experimental Section), whereas the crosses mark measurement values that did not reach the equilibrium within the allowed time limit (48 h). The encircled numbers indicate the order of subsequent (de)sorption cycles. The forms noted in parentheses were identified as minor components by XRPD.

spiked with 1−2% of both Forms I and II° before subjection to moisture sorption/desorption cycles. The desorption curve is similar to that of phase pure Hy2 (Figure 7c). The water is released at RH < 25%, and the product contains Forms I and II° from the spiking and Form III as the dehydration product. Upon subsequently increasing the RH of the mixed anhydrate sample, hydration of Form III to Hy2 is observed as well as a transformation to Form II° (Figure 16, 2). The latter, which is indicated by the decrease in mass despite increasing the humidity at RH values >85%, is consistent with the greater

stability (lower solubility) of Form II° than Hy2 observed in 1:1 acetonitrile/water ($a_w \approx 0.9$), Figure 15.

3.6.3. pH Stability. To investigate the influence of pH on the DB7/DB7[z] form stability, slurry experiments were conducted in aqueous buffer solutions at 25 °C. Solvent mediated transformations (SMT) starting from Hy2/Form III showed that HyA is obtained if pH ≥ 6 and anhydrous Form II° if pH ≤ 5. In contrast, the phosphate salt of DB7 was shown to disproportionate in aqueous media, causing either Hy2 (pH 6−7.8) or Form II° (pH 2.8−5) to nucleate.[47] The fact that Hy2 converted to HyA in the higher pH SMT experiments confirms that Hy2 was a kinetic disproportionation product at 25 °C. Thus, HyA is the thermodynamically most stable DB7[z] form in water, but this stability relationship has been established only at pH ≥ 5.9 (from water slurry experiments).

4. DISCUSSION

DB7 has a rich solid form landscape composed of three neat polymorphs, two hydrates, three solvates, and an amorphous phase. With the goal of exploring the thermodynamic stability relationships between the hydrates and anhydrates, as well as their interconversion pathways, we have established through a combination of diverse experimental techniques and computational chemistry that DB7 form appearance and stability depend on temperature, water activity, and pH. Form II° is monotropically more stable than Forms I, III, and Hy2 and usually more stable than HyA. HyA is the most stable DB7 crystal form in saturated water solutions, but only at pH ≥ 5.9.

Characterizing the structure−stability relationships of the DB7 crystal forms was complicated not only by the difficulty in isolating highly crystalline, phase pure samples of the metastable forms (Section 3.1), but also the slow rate at which HyA and Hy2/Form III materials reached their equilibrium moisture content. Equilibrium water contents were attainable for HyA using extended equilibration times at most RHs, although complete rehydration to full crystallographic water occupancy was never achieved even in aqueous slurries. In contrast, the reversible dehydration of Hy2 to Form III mediated by water vapor was readily apparent from a quick measurement of the moisture sorption−desorption isotherms of either form, yet extended equilibration times did little to minimize the hysteresis (Figure 7c) caused by slow transformation kinetics. The slow interconversion of Hy2 and Form III in the solid state at moderate RHs frustrated attempts to establish the critical water activity relating these metastable forms.

4.1. What Molecular-Level Understanding of Dehydration Mechanisms Has Emerged for the DB7[z] Hydrates? Two distinctly different moisture sorption behaviors were established for Hy2 and HyA through detailed characterization of highly crystalline, phase pure samples as a function of water vapor pressure. Curiously, our initial attempts to rationalize the different hygroscopicity of the DB7[z] hydrates in terms of structural features (solvent pockets, channels) common to stoichiometric and nonstoichiometric hydrates yielded anything but expected results. Figure 17 shows the void space (default probe radius = 1.2 Å) created by removing the waters of crystallization from the HyA$_{1.95}$, HyA$_{1.73}$, HyA$_{1.32}$, and Hy2 structures. Counterintuitively, the water accessible voids in nonstoichiometric HyA appear to be isolated from one another (Figure 17a−c), while water channels are clearly seen running zigzag along the crystallographic *b*-axis in the stoichiometric hydrate, Hy2 (Figure 17d).
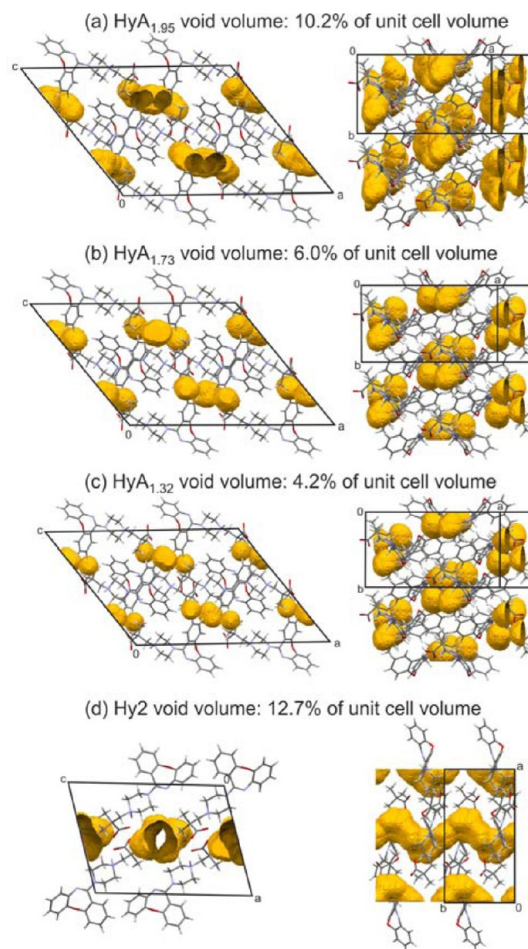

Figure 17. Solvent accessible voids containing waters of crystallization in (a) HyA$_{1.95}$, (b) HyA$_{1.73}$, (c) HyA$_{1.32}$, and (d) Hy2, calculated using a 1.2 Å probe radius.

Cursory inspection of the water channels in Hy2 and the proximity of solvent pockets in HyA suggests that the direction of water ingress/egress is likely to be along the *b*-axis in each structure. However, the 100 K structures individually do not reveal how either hydrate framework would respond to perturbations in RH, particularly at crystallization processing and storage relevant temperatures. Water vapor sorption isotherms (Figure 7), however, show that the DB7[z]/water stoichiometry is retained across a wide RH range for Hy2 and that a fraction of the water in HyA is adventitious. Yet they reveal little as to how water is held in each crystal structure or the phase transformations that accompany dehydration and rehydration. Indeed, only through a combination of experiment and computation were we able to paint a molecular level picture of two very different RH stability profiles and (de)hydration mechanisms for Hy2 and HyA.

Nonstoichiometric HyA retains between 1.29 and 1.95 waters of crystallization, all of which reside in the same solvent pockets in the crystal structure (Figure 17a−c) and are exchangeable (Figure 11b,c). The conspicuous absence of continuous water channels in HyA suggests that for nonstoichiometric hydration to occur, cooperative movement of the carboxylate and dibenzoxepine groups (Figures 9d−f and 17b−c) must temporarily open up diffusion pathways, similar to that seen in β-cyclodextrin (β-CD) hydrate[95] and ciprofloxacin.[96] Water diffusion in and out of discrete

crystallographic sites gives rise to varying disorder and occupancy in the diffraction time-averaged HyA crystal structures, but is sufficiently rapid, at least under moderate to high RH conditions, that single, "averaged" DB7^z ^{13}C resonances are seen in the SSNMR spectra (Figure 10a). Below 11% RH, water mobility is observably decreased with the resonances of ^{13}C nuclei that are in close proximity to the partially occupied water sites showing splitting (Figure 10b). The decrease in water mobility witnessed on the SSNMR time scale at low RH is presumably caused by anisotropic contraction of the HyA lattice as water is continuously lost from the crystal. In fact, Rietveld refinement of the HyA XRPD patterns collected across a wide RH range confirmed that the HyA lattice essentially breathes to accommodate varying amounts of water with smooth changes in the cell volume and shifting of the water sites/occupancies (Figure 9).

Void space analysis of the HyA framework structures derived from HyA$_{1.95}$, HyA$_{1.73}$, and HyA$_{1.32}$ showed that as the unit cell contracts at lower hydration states (Figure 17a−c), the solvent accessible voids decrease from 10.2% in HyA$_{1.95}$ to 4.2% in HyA$_{1.32}$. Isostructural dehydration modeling, in showing the small energy penalty that is incurred to attain full water site occupancy (hemipentahydrate stoichiometry) and the appreciably larger one for decreasing the water content below 1.25 mol equiv in the HyA crystal structure, helped to rationalize the DB7^z/water stoichiometries that were experimentally accessible. In the end, elevated temperatures or long-time storage over P$_2$O$_5$ (0% RH) was required to overcome the activation energy for removing the final 1.3 equiv of water from the contracted HyA structure. However, with no clear path to an appreciably stable neat polymorph, dehydration led to structural collapse as first observed by DSC (Figure 12b), then later confirmed by Raman spectroscopy (Figure 13c).

In contrast to HyA, Hy2 retains its full complement of water over a large RH range at 25 °C (Figure 7c). Stoichiometric hydration may not have been anticipated based on the location of water molecules in open channels in the Hy2 crystal structure, but it was suggested by computational dehydration modeling (Section 3.4.2). In revealing a significant energy penalty incurred by removing water molecules from this hydrate, lattice energy calculations for Hy2 and hypothetical lower hydrate and framework structures derived from Hy2 suggested that even partial dehydration to a lower isostructural hydrate would be highly unlikely. The inability to dehydrate Hy2 (without inducing a phase change) cannot be taken to mean that water exchange in this channel hydrate is not possible, however. In fact, water mobility was found to be similar in Hy2 and HyA by Raman using H$_2$O/D$_2$O exchange (Figure 11a, for details see Section 9 of the Supporting Information).

That water is able to rapidly enter and leave the open channels in Hy2 naturally raises the question: why is the stoichiometry of this hydrate conserved over such a wide RH range? The answer lies in how the Hy2 crystal structure responds to the loss of water. In this case, the Hy2 framework, apparently incapable of making the type of adjustment that HyA makes to accommodate appreciably lower amounts of water, experiences a significant increase in free volume on dehydration. The decreased packing efficiency, along with the loss of strong intermolecular water⋯DB7^z hydrogen bonds, is considerably destabilizing. As a result, Hy2 retains its full complement of water under most RH conditions at ambient temperature. With even modest increases in temperature

(Figure 13) or decreases in RH (Figure 7c), however, Hy2 gives way exclusively to a neat form (Form III). The path to Form III, a neat polymorph that is more efficiently packed than the isomorphic dehydrate, is conceivably paved by the DB7^z conformations that allow intramolecular hydrogen bonding seen in the parent Hy2 structure to be conserved (after proton transfer). Some of the propionic acid side chains in DB7^z undergo a significant conformational change on loss of water from Hy2, leading to a disordered Form III structure. This change probably accounts for the large RH range of coexistence, i.e., hysteresis in the moisture sorption−desorption isotherms measured at 25 °C.

4.2. Does Such Detailed Characterization of Pharmaceutical Hydrates Help to Avoid Problems in Drug Development?
Efficient and reversible nonstoichiometric hydration may be rationalized, and in favorable cases (e.g., cromolyn sodium,[29] AMG 222 tosylate,[97] and Pfizer's glycogen phosphorylase inhibitor[98]), anticipated for open channel structures; however, the hydrates of DB7 highlight the dangers of inferring stoichiometric vs nonstoichiometric hydration from general structural features.[99] The moisture sorption properties of HyA may be unconventional, but they are not unprecedented. Other carefully studied systems, such as topotecan HCl,[100] paroxetine HCl Form II,[28] GSK's ApoA-1 up-regulator,[101] ciprofloxacin,[96] thiamine HCl,[52,102] and β-CD,[95] show a similar ability to equilibrate with the humidity of their surroundings despite lacking continuous channels. However, Hy2 is unusual in its ability to retain stoichiometric amounts of water in open water channels over such a large RH range. Clearly, with neither hydrate behaving according to the conventional classifications based on either structure or absorption isotherms, jumping to conclusions about the hydration behavior from a few hasty experiments would have been very misleading.

Having a molecular level understanding of how water vapor is sorbed in hygroscopic materials and the risks that water uptake poses to the physical and chemical stability of a pharmaceutical product is invaluable, particularly early in drug development when the solid-state form is selected. As some sources of water uptake are more manageable than others, careful evaluation of the stoichiometry, stability relationships, and transformation pathways of pharmaceutical hydrates should inform the solid form screening and selection process. Nonstoichiometric hydration, for example, is an intrinsic and generally undesirable property of a solid form that, once established, might prompt further solid form screening and ultimately would have to be managed in the event that an alternate, nonhygroscopic form is not found. However, water uptake in the amorphous components of poorly crystalline materials is oftentimes correctable with improvements in crystallinity that are generally realized during crystallization process optimization.

Hygroscopicity is, of course, but one of many considerations taken in the selection of a crystal form for a commercial drug product. Perhaps more important to delivering a drug safely and efficaciously are the solubility and stability, both thermodynamic and kinetic, of the solid-state form. As metastable forms of the 5-HT$_{2a}$ and H$_1$ inverse agonist, Hy2 and HyA offer the advantage of generally higher solubility, which might be desirable for ensuring rapid oral delivery of an insomnia medication. However, from a manufacturability and control perspective, the added risk of form conversions established in our assessment of the structure−stability

relationships would have to be carefully weighed in the selection of either of these high energy forms for a commercial drug product. In this case, the difficulties we encountered with producing the DB7 hydrates at small scale and avoiding conversions to the more stable neat forms prompted further evaluation of salt and cocrystal options to determine whether these were better suited for enabling a drug product.

The computational modeling of static structures derived from the time and spatially averaged crystal structures supports the interpretation of the experimental results and accounts for the variability in disorder and water mobility shown by SSNMR and Raman H_2O/D_2O exchange. However, current state-of-the-art calculations still struggle to obtain sufficient accuracy for the small energy differences involved[103] and cannot include the important effects of water activity or temperature, let alone proton-transfer energies. Ideally, we would wish to simulate the nonstoichiometric HyA at ambient temperature to confirm how the water moves and determine the correlated motions within the DB7^z framework (cf. GSK's ApoA-1 up-regulator[101]). Nonetheless, by combining such a range of experimental and appropriate computational work to get a coherent molecular understanding of this complex hydrate/anhydrate system, we show both the potential of computational chemistry for corroborating and assisting in an experimental program, as well as the need for further developments.

5. CONCLUSIONS

A polymorphic system, 3-(4-dibenzo[b,f][1,4]oxepin-11-yl-piperazin-1-yl)-2,2-dimethylpropanoic acid, has two zwitterionic hydrate phases with disordered water, which differ remarkably in stability and hydration/dehydration mechanisms. The full multidisciplinary investigation of the behavior of the hydrate and anhydrate phases was complicated by the difficulty in isolating highly crystalline, phase pure samples, the sluggish equilibration of the hydrates at different RH, the metastability of the various forms at different conditions, and the variable hydration state of HyA. However, structural based models for both hydrates and the metastable Form III rationalize this behavior. This system exemplifies the dangers in assuming behaviors based on cursory observation of stoichiometric and nonstoichiometric hydration. Temperature, water activity, and pH determine the stability ranges of the DB7 solid forms, considerably complicating the processing, storage, and handling of this "unconventional" pharmaceutical hydrate system.

ASSOCIATED CONTENT

S Supporting Information

Observed DB7^z conformations, gravimetric moisture sorption/desorption experiments, variable temperature XRPD and Pawley/Rietveld fitting, variable RH SSNMR, dehydration studies of Hy2 (SSNMR), crystal energy calculations (single point and geometry optimizations), and chemical shift calculations. Crystallographic information files are also available from the Cambridge Crystallographic Data Center (CCDC) upon request (http://www.ccdc.cam.ac.uk, CCDC deposition numbers 1063950 (DB7^z, Hy2), 1063951 (DB7^z, HyA$_{1.73}$), and 1063952 (DB7^z, HyA$_{1.95}$). The Supporting Information is available free of charge on the ACS Publications website at DOI: 10.1021/acs.molpharmaceut.5b00357.

AUTHOR INFORMATION

Corresponding Author

*Tel: +43(0)512 507 58653. E-mail: doris.braun@uibk.ac.at.

REFERENCES

(1) Newman, A. W.; Reutzel-Edens, S. M.; Zografi, G. Characterization of the "hygroscopic" properties of active pharmaceutical ingredients. *J. Pharm. Sci.* **2008**, *97* (3), 1047−1059.

(2) Likar, M. D.; Taylor, R. J.; Fagerness, P. E.; Hiyama, Y.; Robins, R. H. The 3′-keto-diol equilibrium of trospectomycin sulfate bulk drug and freeze-dried formulation: solid-state carbon-13 cross-polarization magic angle spinning (CP/MAS) and high-resolution carbon-13 nuclear magnetic resonance (NMR) spectroscopy studies. *Pharm. Res.* **1993**, *10* (1), 75−79.

(3) Griesser, U. J. The importance of solvates. In *Polymorphism: In the Pharmaceutical Industry*, Hilfiker, R., Ed.; Wiley-VCH: Germany, 2006; pp 211−233.

(4) Braun, D. E. Crystal Polymorphism of Drug Compounds: Statistical Aspects, Analytical Strategies and Case Studies. PhD Thesis, University of Innsbruck. 2008.

(5) Vippagunta, S. R.; Brittain, H. G.; Grant, D. J. W. Crystalline solids. *Adv. Drug Deliver. Rev.* **2001**, *48* (1), 3−26.

(6) Braun, D. E.; Gelbrich, T.; Kahlenberg, V.; Griesser, U. J. Insights into Hydrate Formation and Stability of Morphinanes from a Combination of Experimental and Computational Approaches. *Mol. Pharmaceutics* **2014**, *11*, 3145−3163.

(7) Byrn, S. R.; Pfeiffer, R. R.; Stowell, J. G. *Solid-State Chemistry of Drugs*; second ed.; West Lafayette, IN: SSCI, Inc.1999, West Lafayette, IN.

(8) Zhu, H.; Yuen, C.; Grant, D. J. W. Influence of water activity in organic solvent + water mixtures on the nature of the crystallizing drug phase. 1. Theophylline. *Int. J. Pharm.* **1996**, *135* (1,2), 151−160.

(9) Fucke, K.; McIntyre, G. J.; Lemee-Cailleau, M. H.; Wilkinson, C.; Edwards, A. J.; Howard, J. A. K.; Steed, J. W. Insights into the Crystallisation Process from Anhydrous, Hydrated and Solvated Crystal Forms of Diatrizoic Acid. *Chem. - Eur. J.* **2015**, *21* (3), 1036−1047.

(10) Jeffrey, G. A. Water structure in organic hydrates. *Acc. Chem. Res.* **1969**, *2* (11), 344−352.

(11) Clark, J. R. Water molecules in hydrated organic crystals. *Rev. Pure Appl. Chem.* **1963**, *13*, 50−90.

(12) Brittain, H. G.; Morris, K. R.; Boerrigter, S. X. M. Structural aspects of solvatomorphic systems. In *Polymorphism in Pharmaceutical Solids*, Brittain, H. G., Ed.; Informa Healthcare: New York, 2009; pp 233−281.

(13) Gal, S. Phenomenological study of water vapor sorption isotherms of solid sorbents. *Chimia* **1968**, *22* (11), 409−425.

(14) Authelin, J. R. Thermodynamics of non-stoichiometric pharmaceutical hydrates. *Int. J. Pharm.* **2005**, *303* (1−2), 37−53.

(15) Morris, K. R.; Rodriguez-Hornedo, N. Hydrates. In *Encyclopedia of Pharmaceutical Technology*, Swarbrick, J., Boylan, J., Eds.; Marcel Dekker: New York, 1993; pp 393−440.

(16) Nyqvist, H. Saturated salt solutions for maintaining specified relative humidities. *Int. J. Pharm. Technol. Prod. Manuf.* **1983**, *4* (2), 47−48.

(17) Stubberud, L.; Arwidsson, H. G.; Graffner, C. Water-solid interactions: I. A technique for studying moisture sorption/desorption. *Int. J. Pharm.* **1995**, *114* (1), 55−64.

(18) Roberts, A. The design of an automatic system for the gravimetric measurement of water sorption. *J. Therm. Anal. Calorim.* **1999**, *55* (2), 389−396.

(19) Stephenson, G. A.; Groleau, E. G.; Kleemann, R. L.; Xu, W.; Rigsbee, D. R. Formation of Isomorphic Desolvates: Creating a Molecular Vacuum. *J. Pharm. Sci.* **1998**, *87* (5), 536−542.

(20) Mimura, H.; Kitamura, S.; Kitagawa, T.; Kohda, S. Characterization of the non-stoichiometric and isomorphic hydration and solvation in FK041 clathrate. *Colloids Surf., B* **2002**, *26* (4), 397−406.

(21) Khankari, R. K.; Grant, D. J. W. Pharmaceutical Hydrates. *Thermochim. Acta* **1995**, *248*, 61−79.

(22) Malaj, L.; Censi, R.; Gashi, Z.; Di, M. P. Compression behaviour of anhydrous and hydrate forms of sodium naproxen. *Int. J. Pharm.* **2010**, *390* (2), 142−149.

(23) Zhang, G. G. Z.; Law, D.; Schmitt, E. A.; Qiu, Y. Phase transformation considerations during process development and manufacture of solid oral dosage forms. *Adv. Drug Delivery Rev.* **2004**, *56* (3), 371−390.

(24) Phadnis, N. V; Suryanarayanan, R. Polymorphism in anhydrous theophylline–implications on the dissolution rate of theophylline tablets. *J. Pharm. Sci.* **1997**, *86* (11), 1256−1263.

(25) Raijada, D.; Bond, A. D.; Larsen, F. H.; Cornett, C.; Qu, H.; Rantanen, J. Exploring the Solid-Form Landscape of Pharmaceutical Hydrates: Transformation Pathways of the Sodium Naproxen Anhydrate-Hydrate System. *Pharm. Res.* **2013**, *30* (1), 280−289.

(26) Braga, D.; Grepioni, F.; Chelazzi, L.; Campana, M.; Confortini, D.; Viscomi, G. C. The structure-property relationship of four crystal forms of rifaximin. *CrystEngComm* **2012**, *14* (20), 6404−6411.

(27) Bernardes, C. E. S.; da Piedade, M. E. M. Crystallization of 4′-Hydroxyacetophenone from Water: Control of Polymorphism via Phase Diagram Studies. *Cryst. Growth Des.* **2012**, *12* (6), 2932−2941.

(28) Pina, M. F.; Pinto, J. F.; Sousa, J. J.; Fabian, L.; Zhao, M.; Craig, D. Q. M. Identification and Characterization of Stoichiometric and Nonstoichiometric Hydrate Forms of Paroxetine HCl: Reversible Changes in Crystal Dimensions as a Function of Water Absorption. *Mol. Pharmaceutics* **2012**, *9* (12), 3515−3525.

(29) Stephenson, G. A.; Diseroad, B. A. Structural relationship and desolvation behavior of cromolyn, cefazolin and fenoprofen sodium hydrates. *Int. J. Pharm.* **2000**, *198* (2), 167−177.

(30) Berzins, A.; Skarbulis, E.; Rekis, T.; Actins, A. On the Formation of Droperidol Solvates: Characterization of Structure and Properties. *Cryst. Growth Des.* **2014**, *14* (5), 2654−2664.

(31) Rager, T.; Geoffroy, A.; Hilfiker, R.; Storey, J. M. D. The crystalline state of methylene blue: a zoo of hydrates. *Phys. Chem. Chem. Phys.* **2012**, *14* (22), 8074−8082.

(32) Kumar, S. S.; Nangia, A. A Solubility Comparison of Neutral and Zwitterionic Polymorphs. *Cryst. Growth Des.* **2014**, *14* (4), 1865−1881.

(33) Braun, D. E.; Bhardwaj, R. M.; Florence, A. J.; Tocher, D. A.; Price, S. L. Complex Polymorphic System of Gallic Acid-Five Monohydrates, Three Anhydrates, and over 20 Solvates. *Cryst. Growth Des.* **2013**, *13* (1), 19−23.

(34) Khankari, R.; Chen, L.; Grant, D. J. W. Physical Characterization of Nedocromil Sodium Hydrates. *J. Pharm. Sci.* **1998**, *87* (9), 1052−1061.

(35) Tian, F.; Qu, H.; Zimmermann, A.; Munk, T.; Joergensen, A. C.; Rantanen, J. Factors affecting crystallization of hydrates. *J. Pharm. Pharmacol.* **2010**, *62* (11), 1534−1546.

(36) Gardner, G. L. Kinetics of the dehydration of calcium oxalate trihydrate crystals in aqueous solution. *J. Colloid Interface Sci.* **1976**, *54* (2), 298−310.

(37) Allen, P. V.; Rahn, P. D.; Sarapu, A. C.; Vanderwielen, A. J. Physical characterization of erythromycin: anhydrate, monohydrate, and dihydrate crystalline solids. *J. Pharm. Sci.* **1978**, *67* (8), 1087−1093.

(38) Shibata, M.; Kokubo, H.; Morimoto, K.; Morisaka, K.; Ishida, T.; Inoue, M. X-ray structural studies and physicochemical properties of cimetidine polymorphism. *J. Pharm. Sci.* **1983**, *72* (12), 1436−1442.

(39) Wu, L. S.; Gerard, C.; Koval, C.; Rowe, S.; Hussain, M. A. Crystallinity, hygroscopicity and dissolution of moricizine hydrochloride hemihydrate. *J. Pharm. Biomed. Anal.* **1994**, *12* (8), 1043−1046.

(40) Reutzel-Edens, S. M.; Kleemann, R. L.; Lewellen, P. L.; Borghese, A. L.; Antoine, L. J. Crystal forms of LY334370 HCl: Isolation, solid-state characterization, and physicochemical properties. *J. Pharm. Sci.* **2003**, *92* (6), 1196−1205.

(41) Petrova, R. I.; Peresypkin, A.; Mortko, C. J.; McKeown, A. E.; Lee, J.; Williams, J. M. Rapid conversion of API hydrates to anhydrous forms in aqueous media. *J. Pharm. Sci.* **2009**, *98* (11), 4111−4118.

(42) Stephenson, G. A.; Kendrick, J.; Wolfangel, C.; Leusen, F. J. Symmetry Breaking: Polymorphic Form Selection by Enantiomers of the Melatonin Agonist and Its Missing Polymorph. *Cryst. Growth Des.* **2012**, *12* (8), 3964−3976.

(43) Katdare, A. V.; Bavitz, J. F. Hydrate related dissolution characteristics of norfloxacin. *Drug Dev. Ind. Pharm.* **1984**, *10* (5), 789−807.

(44) Puigjaner, C.; Barbas, R.; Portell, A.; Font-Bardia, M.; Alcobe, X.; Prohens, R. Revisiting the Solid State of Norfloxacin. *Cryst. Growth Des.* **2010**, *10* (7), 2948−2953.

(45) Hu, T. C.; Wang, S. L.; Chen, T. F.; Lin, S. Y. Hydration-induced proton transfer in the solid state of norfloxacin. *J. Pharm. Sci.* **2002**, *91* (5), 1351−1357.

(46) Chongcharoen, W.; Byrn, S. R.; Sutanthavibul, N. Solid state interconversion between anhydrous norfloxacin and its hydrates. *J. Pharm. Sci.* **2008**, *97* (1), 473−489.

(47) Braun, D. E.; McMahon, J. A.; Koztecki, L. H.; Price, S. L.; Reutzel-Edens, S. M. Contrasting Polymorphism of Related Small Molecule Drugs Correlated and Guided by the Computed Crystal Energy Landscape. *Cryst. Growth Des.* **2014**, *14* (4), 2056−2072.

(48) Stahl, P. H.; Wermuth, C. G. *Handbook of Pharmaceutical Salts: Properties, Selection, and Use*; Wiley-VCH: 2002.

(49) Bis, J. A.; Boyle, P. D.; Carino, S. A. R.; Igo, D. H.; Katrincic, L. M. Crystallization and Solid-State Characterization of the Hemihydrate of Albuterol Hemisulfate. *Cryst. Growth Des.* **2014**, *14* (2), 775−782.

(50) Fujii, K.; Aoki, M.; Uekusa, H. Solid-State Hydration/Dehydration of Erythromycin A Investigated by ab Initio Powder X-ray Diffraction Analysis: Stoichiometric and Nonstoichiometric Dehydrated Hydrate. *Cryst. Growth Des.* **2013**, *13* (5), 2060−2066.

(51) Zencirci, N.; Gstrein, E.; Langes, C.; Griesser, U. J. Temperature- and moisture-dependent phase changes in crystal forms of barbituric acid. *Thermochim. Acta* **2009**, *485* (1−2), 33−42.

(52) Te, R. L.; Griesser, U. J.; Morris, K. R.; Byrn, S. R.; Stowell, J. G. X-ray Diffraction and Solid-State NMR Investigation of the Single-Crystal to Single-Crystal Dehydration of Thiamine Hydrochloride Monohydrate. *Cryst. Growth Des.* **2003**, *3* (6), 997−1004.

(53) Berzins, A.; Skarbulis, E.; Rekis, T.; Actins, A. On the Formation of Droperidol Solvates: Characterization of Structure and Properties. *Cryst. Growth Des.* **2014**, *14* (5), 2654−2664.

(54) Braun, D. E.; Karamertzanis, P. G.; Price, S. L. Which, if any, hydrates will crystallise? Predicting hydrate formation of two dihydroxybenzoic acids. *Chem. Commun.* **2011**, *47* (19), 5443−5445.

(55) Braun, D. E.; Tocher, D. A.; Price, S. L.; Griesser, U. J. The Complexity of Hydration of Phloroglucinol: A Comprehensive Structural and Thermodynamic Characterization. *J. Phys. Chem. B* **2012**, *116* (13), 3961−3972.

(56) Stokes, S. P.; Seaton, C. C.; Eccles, K. S.; Maguire, A. R.; Lawrence, S. E. Insight into the Mechanism of Formation of Channel Hydrates via Templating. *Cryst. Growth Des.* **2014**, *14* (3), 1158−1166.

(57) *SAINT: Program for Integration of Area Detector Data*, version 6.2; Bruker AXS: Madison WI, USA, 2001.

(58) Farrugia, L. WinGX suite for small-molecule single-crystal crystallography. *J. Appl. Crystallogr.* **1999**, *32* (4), 837−838.

(59) Burla, M. C.; Caliandro, R.; Camalli, M.; Carrozzini, B.; Cascarano, G. L.; Giacovazzo, C.; Mallamo, M.; Mazzone, A.; Polidori, G.; Spagna, R. SIR2011: a new package for crystal structure determination and refinement. *J. Appl. Crystallogr.* **2012**, *45* (2), 357−361.

(60) Sheldrick, G. M. A short history of SHELX. *Acta Crystallogr., Sect. A* **2008**, *64* (1), 112−122.

(61) Markvardsen, A. J.; David, W. I. F.; Johnson, J. C.; Shankland, K. A probabilistic approach to space-group determination from powder diffraction data. *Acta Crystallogr., Sect. A* **2001**, *57*, 47−54.

(62) David, W. I. F.; Shankland, K.; van de Streek, J.; Pidcock, E.; Motherwell, W. D. S.; Cole, J. C. DASH: a program for crystal structure determination from powder diffraction data. *J. Appl. Crystallogr.* **2006**, *39*, 910−915.

(63) Pawley, G. S. Unit-Cell Refinement from Powder Diffraction Scans. *J. Appl. Crystallogr.* **1981**, *14* (DEC), 357−361.

(64) Rietveld, H. M. A Profile Refinement Method for Nuclear and Magnetic Structures. *J. Appl. Crystallogr.* **1969**, *2*, 65−71.

(65) *Topas Academic V5*, Coelho Software: Brisbane, 2012.

(66) Ahlqvist, M. U. A.; Taylor, L. S. Water diffusion in hydrated crystalline and amorphous sugars monitored using H/D exchange. *J. Pharm. Sci.* **2002**, *91* (3), 690−698.

(67) Martens, H.; Naes, T. *Multivariate Calibration*; Wiley VCH: Chichester, 1991.

(68) Roggo, Y.; Chalus, P.; Maurer, L.; Lema-Martinez, C.; Edmond, A.; Jent, N. A review of near infrared spectroscopy and chemometrics in pharmaceutical technologies. *J. Pharm. Biomed. Anal.* **2007**, *44* (3), 683−700.

(69) Jorgensen, A. C.; Miroshnyk, I.; Karjalainen, M.; Jouppila, K.; Siiria, S.; Antikainen, O.; Rantanen, J. Multivariate data analysis as a fast tool in evaluation of solid state phenomena. *J. Pharm. Sci.* **2006**, *95* (4), 906−916.

(70) Fung, B. M.; Khitrin, A. K.; Ermolaev, K. *J. Magn. Reson.* **2000**, *142*, 97−101.

(71) Antzutkin, O. N. Sideband manipulation in magic-angle-spinning nuclear magnetic resonance. *Prog. Nucl. Magn. Reson. Spectrosc.* **1999**, *35* (3), 203−266.

(72) Metz, G.; Wu, X. L.; Smith, S. O. *J. Magn. Reson. A* **1994**, *110*, 219−227.

(73) Clark, S. J.; Segall, M. D.; Pickard, C. J.; Hasnip, P. J.; Probert, M. J.; Refson, K.; Payne, M. C. First principles methods using CASTEP. *Z. Kristallogr.* **2005**, *220* (5−6), 567−570.

(74) Perdew, J. P.; Burke, K.; Ernzerhof, M. Generalized gradient approximation made simple. *Phys. Rev. Lett.* **1996**, *77* (18), 3865−3868.

(75) Vanderbilt, D. Soft Self-Consistent Pseudopotentials in a Generalized Eigenvalue Formalism. *Phys. Rev. B* **1990**, *41* (11), 7892−7895.

(76) Tkatchenko, A.; Scheffler, M. Accurate Molecular Van Der Waals Interactions from Ground-State Electron Density and Free-Atom Reference Data. *Phys. Rev. Lett.* **2009**, *102* (7), 073005−1−073005/4.

(77) Grimme, S. Semiempirical GGA-type density functional constructed with a long-range dispersion correction. *J. Comput. Chem.* **2006**, *27* (15), 1787−1799.

(78) Griffiths, G. I. G.; Misquitta, A. J.; Fortes, A. D.; Pickard, C. J.; Needs, R. J. High pressure ionic and molecular crystals of ammonia monohydrate within density functional theory. *J. Chem. Phys.* **2012**, *137* (6), 064506−1−064506/9.

(79) Thierfelder, C.; Hermann, A.; Schwerdtfeger, P.; Schmidt, W. G. Strongly bonded water monomers on the ice Ih basal plane: Density-functional calculations. *Phys. Rev. B: Condens. Matter Mater. Phys.* **2006**, *74* (4), 045422−1−045422/5.

(80) Beran, G. J. O.; Nanda, K. Predicting Organic Crystal Lattice Energies with Chemical Accuracy. *J. Phys. Chem. Lett.* **2010**, *1* (24), 3480−3487.

(81) Pickard, C. J.; Mauri, F. All-electron magnetic response with pseudopotentials: NMR chemical shifts. *Phys. Rev. B: Condens. Matter Mater. Phys.* **2001**, *63* (24), 245101−1−245101/13.

(82) Etter, M. C.; MacDonald, J. C.; Bernstein, J. Graph-Set Analysis of Hydrogen-Bond Patterns in Organic- Crystals. *Acta Crystallogr., Sect. B* **1990**, *46*, 256−262.

(83) Mohamed, S.; Tocher, D. A.; Vickers, M.; Karamertzanis, P. G.; Price, S. L. Salt or cocrystal? A new series of crystal structures formed from simple pyridines and carboxylic acids. *Cryst. Growth Des.* **2009**, *9* (6), 2881−2889.

(84) Li, X.; Bond, A. D.; Johansson, K. E.; van de Streek, J. Distinguishing tautomerism in the crystal structure of (Z)-N-(5-ethyl-2,3-dihydro-1,3,4-thiadiazol-2-ylidene)-4-methylbenzenesulfonamide using DFT-D calculations and 13C solid-state NMR. *Acta Crystallogr., Sect. C* **2014**, *70* (8), 784−789.

(85) Kontny, M. J.; Zografi, G. Sorption of water by solids. In *Physical Characterization of Pharmaceutical Solids*, 70 ed.; Brittain, H. G., Ed.; Marcel Dekker: New York, 1995; pp 387−418.

(86) PLATON[87] analysis confirmed that *c*Hy2 was still consistent with both the experimental $P2_1/c$, Z′=1 symmetry and the proton disorder over two positions with an occupancy factor of 0.5.

(87) *PLATON, A Multipurpose Crystallographic Tool*, Utrecht University: Utrecht, The Netherlands, 2003.

(88) Ignoring proton positions.

(89) It is well-known that the functional overestimates water···water interactions but as the same type of interactions are present in the hydrate structures we decided to use the lattice energy for ice XI as a reference energy.

(90) Harris, R. K. Applications of solid-state NMR to pharmaceutical polymorphism and related matters. *J. Pharm. Pharmacol.* **2007**, *59* (2), 225−239.

(91) The measurements, using an open pan, were started immediately after exposing the sample to N_2. Furthermore, the measurements were repeated in a pan that was covered with a one pin-holed lid to slow down the starting of the dehydration process. The results of both measurement methods were in agreement.

(92) Kuhnert-Brandstaetter, M.; Proell, F. Thermal analysis of hydrates of organic compounds. II. *Mikrochim. Acta* **1983**, *3* (5−6), 287−300.

(93) For hot-stage thermomicroscopic investigations a Reichert Thermovar polarization microscope equipped with a Kofler hot-stage (Reichert, A) was used.

(94) Goelles, F. The examination and calculation of thermodynamic data from experimental measurements. I. The numerical integration of the vapor-pressure curves of the system methanol-water. *Monatsh. Chem.* **1961**, *92*, 981−991.

(95) Steiner, T.; Koellner, G. Crystalline β-Cyclodextrin Hydrate at Various Humidities: Fast, Continuous, and Reversible Dehydration Studied by X-ray Diffraction. *J. Am. Chem. Soc.* **1994**, *116* (12), 5122−5128.

(96) Mafra, L.; Santos, S. M.; Siegel, R.; Alves, I.; Almeida Paz, F. A.; Dudenko, D.; Spiess, H. W. Packing Interactions in Hydrated and Anhydrous Forms of the Antibiotic Ciprofloxacin: a Solid-State NMR, X-ray Diffraction, and Computer Simulation Study. *J. Am. Chem. Soc.* **2012**, *134* (1), 71−74.

(97) Kiang, Y. H.; Cheung, E.; Stephens, P. W.; Nagapudi, K. Structural studies of a nonstoichiometric channel hydrate using high-resolution x-ray powder diffraction, solid-state nuclear magnetic resonance, and moisture Sorption methods. *J. Pharm. Sci.* **2014**, *103* (9), 2809−2818.

(98) Murphy, B. J.; Casteel, M. J.; Samas, B.; Krzyzaniak, J. F. Thermodynamic stability considerations for isostructural dehydrates. *J. Pharm. Sci.* **2012**, *101* (4), 1486−1495.

(99) Barbour, L. J. Crystal porosity and the burden of proof. *Chem. Commun.* **2006**, *11*, 1163−1168.

(100) Vogt, F. G.; Brum, J.; Katrincic, L. M.; Flach, A.; Socha, J. M.; Goodman, R. M.; Haltiwanger, R. C. Physical, Crystallographic, and Spectroscopic Characterization of a Crystalline Pharmaceutical Hydrate: Understanding the Role of Water. *Cryst. Growth Des.* **2006**, *6* (10), 2333−2354.

(101) Kang, F.; Vogt, F. G.; Brum, J.; Forcino, R.; Copley, R. C. B.; Williams, G.; Carlton, R. Effect of Particle Size and Morphology on the Dehydration Mechanism of a Non-Stoichiometric Hydrate. *Cryst. Growth Des.* **2012**, *12* (1), 60−74.

(102) Chakravarty, P.; Berendt, R. T.; Munson, E. J.; Young, J.; Govindarajan, R.; Suryanarayanan, R. Insights into the dehydration behavior of thiamine hydrochloride (vitamin B1) hydrates: part II. *J. Pharm. Sci.* **2010**, *99* (4), 1882−1895.

(103) Gelbrich, T.; Braun, D. E.; Ellern, A.; Griesser, U. J. Four Polymorphs of Methyl Paraben: Structural Relationships and Relative Energy Differences. *Cryst. Growth Des.* **2013**, *13* (3), 1206−1217.